Title:

Target-agnostic identification of human antibodies to *Plasmodium falciparum* sexual forms reveals cross stage recognition of glutamate-rich repeats.

Author List:

Axelle Amen[1,2,*], Randy Yoo[3,4,*], Amanda Fabra-García[5,*], Judith Bolscher[6], William J.R. Stone[7], Isabelle Bally[1], Sebastián Dergan-Dylon[1], Iga Kucharska[3], Roos M. de Jong[5], Marloes de Bruijni[6], Teun Bousema[5], C. Richter King[8], Randall S. MacGill[8], Robert W. Sauerwein[6], Jean-Philippe Julien[3,4,9,#], Pascal Poignard[1,2,10,#], Matthijs M. Jore[5,#]

[1] CNRS, Univ. Grenoble Alpes, CEA, UMR5075, Institut de Biologie Structurale, 38042 Grenoble, France
[2] CHU Grenoble Alpes, 38000 Grenoble, France
[3] Program in Molecular Medicine, The Hospital for Sick Children Research Institute, Toronto, ON, Canada.
[4] Department of Biochemistry, University of Toronto, Toronto, ON, Canada.
[5] Department of Medical Microbiology, Radboudumc, Nijmegen, the Netherlands.
[6] TropIQ Health Sciences, Nijmegen, the Netherlands.
[7] Department of Immunology and Infection, London School of Hygiene and Tropical Medicine, London, United Kingdom.
[8] Center for Vaccine Innovation and Access, PATH, Washington, DC 20001, USA
[9] Department of Immunology, University of Toronto, Toronto, ON, Canada.
[10] Department of Immunology and Microbiology, The Scripps Research Institute, La Jolla, CA 92037, USA.

*contributed equally
#contributed equally and corresponding authors:
Jean-Philippe.Julien@sickkids.ca; Pascal.Poignard@ibs.fr; Matthijs.Jore@radboudumc.nl

Competing Interests Statement:

The authors declare to have no competing interests.

Author Contributions:

A.A., R.Y, A.F-G., J.B. T.B., C.R.K., R.S.M., R.W.S, J-P.J., P.P. and M.M.J. designed research; A.A., R.Y., A.F-G., J.B., W.J.R.S., I.B., S.D-D., I.K., R.M.d.J. and M.d.B. performed research; A.A., R.Y., A.F-G., J.B., W.J.R.S., I.B., S.D-D., I.K., R.M.d.J., M.d.B. R.W.S., J-P.J., P.P. and M.M.J. analyzed data. A.A., R.Y. J-P.J., P.P. and M.M.J. wrote the original draft. All authors reviewed the manuscript.

Abstract:

Circulating sexual stages of *Plasmodium falciparum (Pf)* can be transmitted from humans to mosquitoes, thereby furthering the spread of malaria in the population. It is well established that antibodies (Abs) can efficiently block parasite transmission. In search for naturally acquired Ab targets on sexual stages, we established an efficient method for target-agnostic single B cell activation followed by high-throughput selection of human monoclonal antibodies (mAbs) reactive to sexual stages of *Pf* in the form of gamete and gametocyte extract. We isolated mAbs reactive against a range of *Pf* proteins including well-established targets Pfs48/45 and Pfs230. One mAb, B1E11K, was cross-reactive to various proteins containing glutamate-rich repetitive elements expressed at different stages of the parasite life cycle. A crystal structure of two B1E11K Fab domains in complex with its main antigen, RESA, expressed on asexual blood stages, showed binding of B1E11K to a repeating epitope motif in a head-to-head conformation engaging in affinity-matured homotypic interactions. Thus, this mode of recognition of *Pf* proteins, previously described only for PfCSP, extends to other repeats expressed across various stages. The findings augment our understanding of immune-pathogen interactions to repeating elements of the *Plasmodium* parasite proteome and underscore the potential of the novel mAb identification method used to provide new insights into the natural humoral immune response against *Pf*.

Impact Statement:

A naturally acquired human monoclonal antibody recognizes proteins expressed at different stages of the *Plasmodium falciparum* lifecycle through affinity-matured homotypic interactions with glutamate-rich repeats

Introduction:

The eradication of malaria remains a global health priority. In 2021, 247 million people were diagnosed with malaria with over 619,000 people succumbing to the disease (1). Malaria is caused by *Plasmodium* parasites: unicellular eukaryotic protozoans that transmit to human hosts through an *Anopheles* mosquito vector. Although insecticide-treated nets and various antimalarial compounds have aided in controlling the spread and combating severe clinical complications of the disease, mosquito and parasite strains resistant to such interventions have emerged (2). Thus, there is an urgent need to develop other technologies, such as vaccines, to help combat the spread of malaria, and eventually, contribute to the eradication of the disease.

The development of a highly efficacious malaria vaccine has been challenging, owing to the complex life cycle of malaria-causing parasites. The life cycle of *Plasmodium spp.* can be categorized into three distinct stages: the pre-erythrocytic, asexual blood stage, and sexual stages. Each step features the parasite undergoing large-scale morphological changes accompanied by modifications in proteomic expression profiles – with several proteins being exclusively expressed in a single stage (3). Therefore, vaccine-mediated humoral responses must be robust enough to generate sufficiently high-quality antibody responses to eliminate the majority of parasites at the stage the vaccine targets. As a result, one approach to vaccine development has focused on targeting “bottlenecks” in the parasite's life cycle where the number of parasites is low (4) (5).

The pre-erythrocytic stage – following the transmission of sporozoites to humans by a bite from an infected mosquito – is a bottleneck targeted by the only two malaria vaccines recommended by the World Health Organization, RTS,S/AS01 and R21/Matrix-M (6) (7). The vaccines are based on the circumsporozoite protein (CSP) – an essential protein expressed at high density on the surface of the parasite during the pre-erythrocytic stage (8) (9) (10). In its central domain, the protein contains various four amino acid repeat motifs – the most predominant of those being NANP repeats. Protective antibodies elicited against CSP primarily target this immunodominant repeat region. A large proportion of these antibodies engage in homotypic interactions which are characterized by direct interactions between two antibodies’ variable regions when bound to adjacent repetitive epitopes (11) (12) (13) (14) (15) (16) (17) (18) (19). Such interactions have been demonstrated to augment B cell activation and contribute to shaping the humoral response to CSP (12). Although these first-generation malaria vaccines only induce short-lived efficacy in a subset of the at-risk population (20), they will undoubtedly assist in lowering the overall incidence of malaria in young infants with clear initial impact (21). Modeling suggests that for improvements towards eradication of the disease, combining multiple types of interventions that target different stages of the *Plasmodium* life cycle may strongly increase the efficacy of weaker interventions (22).

Another bottleneck in the parasite’s life cycle occurs during its sexual stage, which takes place in the mosquito vector. This stage begins when intraerythrocytic *Plasmodium* gametocytes, which are capable of eliciting antibody responses through clearance in the spleen (23), are taken up through a mosquito bloodmeal. Once inside the mosquito midgut, gametocytes emerge from erythrocytes and mature into gametes which then undergo fertilization ultimately resulting in the generation of sporozoites that can go on to infect the next human host. Vaccines that aim to target this life cycle bottleneck are known as transmission-blocking vaccines (TBVs) (24). The goal of TBVs is to elicit antibodies that target sexual stage antigens to block the reproduction of the parasite in the mosquito and thus onward transmission to humans. Current TBV development efforts are primarily focused on two antigens, Pfs230 and Pfs48/45, as they are the targets of the most potent transmission-blocking antibodies identified to date (25) (26) (27) (28). Indeed,

individuals with sera enriched in antibodies that target Pfs230 and Pfs48/45 were found to have high transmission-reducing activity (29). Protective responses to Pfs230 and Pfs48/45 are well characterized at a molecular and structural level (26) (27) (28) (30) (31) (32) (33) (34). However, sera depleted in antibodies targeting the pro domain and domain 1 of Pfs230 and domains 2 and 3 of Pfs48/45 can retain transmission-reducing activity while maintaining the ability to recognize the surface of parasites lacking Pfs48/45 and Pfs230 surface expression (29). This highlights the importance of expanding our understanding of antibody responses to other sexual stage antigens.

We designed a workflow for the isolation of Abs to sexual stage specific antigens from a donor who was repeatedly exposed to malaria parasites. Our efforts yielded a panel of 14 monoclonal antibodies (mAbs) targeting Pfs230 and Pfs48/45 as well as other unidentified proteins, some with transmission-reducing activity. One mAb exhibited cross-reactivity to multiple antigens present at various stages of the parasite's life cycle, by targeting glutamate-rich repeats and engaging in homotypic interactions. This latest result underscores a pivotal role of repetitive elements in shaping the humoral response to *Pf.*

Results:

Agnostic memory B cell (MBC) sorting and activation identifies potential *Pf* sexual stage protein-specific mAbs.

We selected donor A, a 69-year-old Dutch expatriate who resided in Central Africa for approximately 30 years and whose serum was shown to strongly reduce *Pf* transmission, to isolate sexual stage-specific mAbs. We previously demonstrated the serum of this donor, donor A, largely retained its transmission-reducing activity (TRA) when depleted of antibodies directed against the main transmission-blocking epitopes of Pfs48/45 and *Pf*s230 (29), suggesting the presence of antibodies targeting other epitopes on these 2 proteins or directed at other proteins also involved in transmission.

PBMCs from the donor were thawed and a total of 1496 IgG+ memory B cells were sorted in 384-well plates **(Fig. 1) (Fig. S1A)**. After activation, single cell culture supernatants potentially containing secreted IgGs were screened in a high-throughput 384-well ELISA for their reactivity against a crude *Pf* gamete lysate **(Fig. S1B)**. A subset of supernatants was also screened against gametocyte lysate **(S1C)**. In total, supernatants from 84 wells reacted with gamete and/or gametocyte lysate proteins, representing 5.6% of the total memory B cells. Of the 21 supernatants that were screened against both gamete and gametocyte lysates, six recognized both, while nine appeared to recognize exclusively gamete proteins, and six exclusively gametocyte proteins**.**

To isolate the corresponding mAbs, single B cell lysates from the 84 ELISA-positive wells were subjected to single B cell reverse transcriptase PCR (RT-PCR) for amplification of immunoglobulin variable genes. We obtained and cloned heavy and light chain sequences for 11 out of 84 wells. For three wells we obtained a kappa light chain sequence and for five wells a lambda light chain sequence. For three wells we obtained both a lambda and kappa light chain sequence suggesting that either both chains were present in a single B cell or that two B cells were present in the well. For all 14 wells we retrieved a single heavy chain sequence. Following amplification and cloning, 14 mAbs were expressed as full human IgG1s **(Table S1) (Dataset S1).** (34)

Isolated mAbs exhibit distinct patterns of recognition of gamete surface proteins.

173 The 14 mAbs were first tested for binding to *Pf* sexual stage surface antigens in a surface immune-
174 fluorescence assay using wild-type female gametes **(Fig. 2A)**. The mAbs were also tested for
175 binding to Pfs48/45 knock-out female gametes, which lack surface-bound Pfs48/45 and Pfs230
176 (35) (29) Seven mAbs exhibited binding to approximatively half or more of gametes when tested
177 at a concentration of 100 µg/ml. Among these, four mAbs, B1C5K, B1C5L, B2C10L and B2E9L,
178 recognized wild-type gametes with high scores (>68%) even at concentrations as low as 1 µg/ml.
179 The binding of the B1C5K, B1C5L, B2C10L and B2E9L mAbs strongly decreased when using
180 gametes that lacked surface-expressed Pfs48/45 and Pfs230, indicating that these four mAbs
181 likely targeted one of these two antigens. Three other mAbs, B2D10L, B1C8L and B1E7K,
182 displayed a similar recognition profile, albeit with notably smaller percentages of labeled wild-type
183 gametes, particularly at the lower concentrations tested. This suggested a potential low affinity
184 recognition of either Pfs48/45 or Pfs230 for these latter three mAbs.
185
186 Six of the remaining seven mAbs, B1C8K , B1D3L, B1D3K, B1F9K, B1C3L, and B2F7L, exhibited
187 very weak or no binding to gametes. For B1C8K, this showed that the light chain (kappa) did not
188 correspond to the antibody that was originally selected in the screening process as the lambda
189 version (B1C8L) exhibited strong binding. As for the other mAbs, the results indicated that they
190 may be specific for proteins not expressed or only poorly expressed at the gamete surface.
191
192 Finally, one mAb, B1E11K, exhibited a distinctive gamete surface binding profile, recognizing only
193 a fraction (approximately a third to a fifth) of the wild-type and Pfs48/45 knock-out gametes across
194 all tested concentrations, suggesting potential binding to non-Pfs48/45 and Pfs230 proteins.
195
196 **Isolated mAbs have varying transmission-reducing activities and recognize different *Pf***
197 **sexual stage proteins.**
198
199 We were interested in investigating potential TRA for all identified mAbs. To do this, a standard
200 membrane feeding assay (SMFA) was conducted in the presence of the isolated mAbs, revealing
201 a range of transmission-reducing activities **(Fig. 2B)(Table S2)**. Overall, seven mAbs were
202 confirmed to strongly reduce transmission (TRA > 80%) when tested at 500 µg/ml: B1C5K,
203 B1C5L, B2C10L, B2E9L, B1C8L, B1D3L and B1F9K. Of those, two mAbs, B1C8L and B2C10L
204 retained >50% TRA at a lower concentration (100 µg/ml). Notably, despite not showing gamete
205 surface recognition, B1F9K and B1D3L displayed TRA – although only at high concentrations.
206 Conversely, three mAbs recognizing the gamete surface, B2D10L, B1E7K and B1E11K, showed
207 no activity in SMFA.
208
209 To gain deeper insight into the specificity of the various isolated mAbs, regardless of their
210 transmission-reducing activity, we conducted further characterization via Western blot analyses
211 using gametocyte extracts **(Fig. 2C)**. The B1C5K and B1C5L mAbs recognized a protein with a
212 molecular weight matching that of Pfs48/45. This result was consistent with the findings from the
213 gamete surface binding experiment in which these mAbs recognized wildtype gametes but not
214 Pfs48/45 knockout gametes, providing further validation of the specificity of the B1C5K and
215 B1C5L mAbs in targeting Pfs48/45. The B2C10L mAb displayed pattern of recognition that
216 corresponded to Pfs230, similar to the anti-Pfs230 control mAb RUPA-96 (26). Once again, these
217 results were in agreement with the findings from the gamete surface binding experiment
218 confirming the specificity of the B2C10L mAb in targeting Pfs230. The B1E11K mAb also
219 appeared to bind to Pfs230 on the Western blot. However, in contrast to the RUPA-96 mAb,
220 B1E11K only recognized the higher molecular band corresponding to Pfs230, suggesting
221 exclusive recognition of the unprocessed form of this protein (36). Interestingly, besides Pfs230,
222 B1E11K also recognized several unidentified proteins ranging from 70 and 250 kDa with various
223 intensities. These findings were consistent with the gamete binding assay that showed

224 recognition of gametes lacking Pfs48/45 and Pfs230, suggesting potential recognition of proteins
225 other than Pfs48/45 and Pfs230. Finally, all the other mAbs showed no clear binding to any protein
226 from the gametocyte extract on the Western blot. In the case of those demonstrating binding to
227 gamete surfaces, B2E9L, B2D10L, B1C8L, B1E7K, this may be attributed to their recognition of
228 conformational epitopes that are lost during Western blotting preparation, or possibly of specific
229 recognition of proteins expressed in gametes but not gametocytes.
230
231 The recognition of Pfs48/45 by the B1C5K and B1C5L mAbs was subsequently confirmed through
232 an ELISA using full-length recombinant Pfs48/45 **(Fig. 2D)**. Notably, none of the other mAbs of
233 the panel displayed binding to this Pfs48/45 recombinant protein construct. To further pinpoint the
234 domain targeted by B1C5K and B1C5L, an ELISA was performed using constructs corresponding
235 to domains 1-2, 2-3 and 3 revealing that these two mAbs targeted Domain 2 of Pfs48/45 **(Fig.**
236 **2E)**. This is in agreement with prior work indicating mAbs to Domain 2 of Pfs48/45 are generally
237 mAbs with low potency (27).
238
239 The combined findings above strongly pointed to Pfs230 as the target of mAb B2C10L. We thus
240 tested this mAb in ELISA for binding to Pfs230CMB, a construct containing Pfs230 domain 1 and
241 part of the pro-domain (37) No reactivity was observed **(Fig. 2F)** suggesting that B2C10L may
242 recognize other Pfs230 domains than the one tested, or recognize epitopes not properly displayed
243 in the construct used.
244
245 In summary, our target-agnostic mAb isolation approach successfully identified mAbs against *Pf*
246 sexual stage proteins, some of which exhibited TRA and some of which target Pfs48/45 or Pfs230.
247 However, given that the mAbs isolated in this study showed substantially lower TRA than mAbs
248 identified previously (38) (39) we elected not to investigate them further. Instead, we were
249 intrigued by the binding properties of B1E11K, which showed cross-reactivity with various *Pf*
250 proteins, including Pfs230. Such cross-reactivity has been shown as a hallmark of the human Ab
251 response to *Pf* and explored at the serum level but to our knowledge has never been studied at
252 the mAb level (40) (41). Thus, we rationalized a more detailed molecular characterization of this
253 mAb may provide insights into this relatively unexplored phenomenon.
254
255 **The B1E11K mAb cross-reacts to distinct sexual and asexual stage *Pf* proteins containing**
256 **glutamate-rich repeats.**
257
258 First, to ensure the ability of B1E11K to recognize different proteins in Western blotting
259 experiments was not due to polyreactivity, the mAb was tested in ELISA against a panel of human
260 proteins, single-stranded DNA (ssDNA) and lipopolysaccharide (LPS). The 4E10 mAb, a well-
261 known anti-HIV gp41 polyreactive mAb (42), was used as a positive control. The B1E11K mAb
262 did not bind any of the antigens on the panel at any significant level, even at a high 50 µg/ml
263 concentration, and therefore polyreactivity was ruled out **(Fig. S2A)**.
264
265 To identify antigens recognized by B1E11K, immunoprecipitation experiments were conducted
266 using gametocyte extract. Proteins of different molecular weights were specifically detected in the
267 B1E11K immunoprecipitate but not when using the anti-HIV control mAb **(Fig. S2B)**. Mass
268 spectrometry analysis of the corresponding gel slices revealed recognition of Pfs230, confirming
269 the Western blot results.
270
271 The specificity of B1E11K was further tested using a protein microarray featuring recombinant
272 proteins corresponding to putative antigens expressed at the sexual stage as well as proteins
273 expressed at different stages of the *Pf* life cycle (29)**.** The results showed that B1E11K exhibited
274 high level reactivity (>8-fold higher than the negative control, minimum signal intensity rank 15th

of 943 array targets) against several antigens, some expressed at the sexual stage (*i.e.* Pf11.1), others at the asexual stage (*i.e.* LSA3, RESA, RESA3) (**Fig. 3A**). Analysis of the primary amino acid sequence of the antigens recognized in the array suggested homology in several cases, based on the presence of glutamate-rich regions **(Fig. S3)**. To analyze the numerous repeated motifs contained in these proteins, we used the RADAR (Rapid Automatic Detection and Alignment of Repeats) software (43). Although B1E11K recognition of Pfs230 fragments on the array was lower than our cut off for further analysis (3.4-fold higher than the negative control, maximum signal intensity rank 30th of 943 array targets), its sequence was also analyzed using RADAR due to its recognition by B1E11K in the immunoprecipitation experiments (**Fig. S4**). The analysis showed Pfs230 and several of the proteins recognized by B1E11K on the array contained diverse patterns of glutamate-rich repeats of different lengths and compositions. Among these proteins, Pfs230, Pf11.1, RESA, RESA3 and LSA3 presented the most similar glutamate repeats, following an "EE-XX-EE" pattern **(Fig. S4)**. Pfs230 contains adjacent EE-VG-EE repeats which are located in the domain of the protein which is cleaved upon gametocyte egress from erythrocytes (44). RESA and RESA3 contain 20 and nine EE-NV-EE overlapping repeats at the C terminus of the protein, respectively. LSA3 contains two overlapping EE-NV-EE repeats. Finally, 221 non-adjacent EE-LV-EE repeats span the whole Pf11.1 megadalton protein.

To verify the recognition of the aforementioned proteins, a Western blot was performed with recombinant forms of RESA, RESA3, LSA3, and of a Pf11.1 domain (45) **(Fig. 3B)**. Domain 1 of Pfs230, which does not contain the EE-VG-EE repeats, was also included. The results confirmed the binding of B1E11K to all the proteins tested except for Pfs230D1, as expected. Overall, the data showed that the B1E11K mAb recognizes various *Pf* proteins from different stages, all containing glutamate-rich repeats.

To validate the B1E11K mAb specifically targets glutamate-rich repeats, we synthesized five biotinylated peptides derived from the various repeats found in the proteins identified above to test for binding in sandwich ELISA experiments **(Fig. 3C)**. Overall, the B1E11K mAb bound to all peptides **(Fig. 3D)**. However, it exhibited a higher specificity for the RESA-derived peptides with an EC_{50} at least 100 times greater compared to EC_{50} values obtained with the other glutamate-rich peptides. Altogether, this suggests the main antigenic targets of B1E11K are RESA and RESA3, which contain the EENV repeats.

Since B1E11K bound to RESA-based peptides the strongest, we synthesized shorter RESA peptides for a more precise determination of the B1E11K minimal sequence epitope **(Fig. 4A)**. When tested on the RESA peptide panel, B1E11K mAb binding to RESA P2 (16AA) and RESA 14AA, 12AA, and 10AA was similar, all exhibiting close EC_{50} values **(Fig. 4B) (Fig. S6)**. No binding was observed for the 8AA RESA peptide, suggesting the 10AA peptide contained the minimal epitope. We hypothesized the similar EC_{50} values may be a result of avidity effects and thus, we performed the same experiment with recombinant B1E11K Fab **(Fig. 4C)**. Although B1E11K Fab bound both RESA P2 (16AA) and RESA 14AA peptides with comparable strength of binding, both RESA 12AA and RESA 10AA peptides displayed comparatively poorer EC_{50} values with the RESA 10AA peptide displaying the lowest detectable binding strength. The binding affinity and kinetics of the interaction was also determined through biolayer interferometry (BLI). We performed experiments using the minimal sequence required for binding determined through ELISA [RESA 10AA peptide and the RESA P2 peptide (16AA)]. When immobilizing the peptide to the sensors, an approximately six-fold difference in affinity between the 10AA peptide (K_D = 484 nM) **(Fig. 4D)** and the P2 peptide (16AA) (K_D = 74 nM) **(Fig. 4E)** was observed.

Four EENV repeats permit two B1E11K Fabs to bind.

326 Given the repetitive nature of the antigenic targets of B1E11K and differences in binding events
327 captured in our BLI experiments, we hypothesized that more than one B1E11K Fab could
328 potentially bind to the longer, RESA P2 (16AA) peptide. Thus, we performed isothermal titration
329 calorimetry using the same two RESA peptides as in the BLI experiments to determine the binding
330 stoichiometries. We observed when titrating the B1E11K Fab into RESA 10AA, a binding
331 stoichiometry of N = 1.0 ± 0.2 **(Fig. 4F) (Table 1)**. When using the RESA P2 (16AA) peptide, a
332 stoichiometry of N = 2.1 ± 0.1 was observed **(Fig. 4G) (Table 1)**. The determined binding affinity
333 from our ITC experiments **(Table 1)** differed from our BLI experiments **(Fig. 4D and 4E)**, which
334 can occur when measuring antibody-peptide interactions (46). Regardless, our data all trend
335 toward the same finding in which a stronger binding affinity is observed toward the longer RESA
336 P2 (16AA) peptide.
337
338 To further corroborate our binding stoichiometry findings, we performed size-exclusion
339 chromatography coupled with multi-angle light scattering (SEC-MALS) to determine the molecular
340 weight of the 2:1 Fab:peptide complex **(Fig. 4H)**. We incubated a molar excess Fab:peptide (6:1)
341 sample to saturate all B1E11K Fab binding sites present on the RESA peptide to obtain a solution
342 containing the putative complex and excess monomeric Fab. The resulting chromatogram
343 revealed two species eluted from the column. The molecular weight of the heavier species was
344 in line with what would be expected from a 2:1 Fab:peptide complex (92 kDa) in which the mass
345 determined fell within the range of experimental error. A negative-stain electron microscopy
346 (nsEM) map reconstruction of the 2:1 Fab:peptide complex recovered from the SEC-MALS
347 experiment **(Fig. 4H)** permitted the fitting of two Fab molecules, further supporting the 2:1 binding
348 model **(Fig. 4I)**.
349
350 **B1E11K binds EENV repeats in a head-to-head conformation leveraging homotypic**
351 **interactions.**
352
353 To obtain a full structural understanding of the observed repeat cross-reactivity and selectivity for
354 RESA exhibited by B1E11K, we solved a 2.6 Å crystal structure of the B1E11K:RESA P2 (16AA)
355 peptide complex **(Fig. 5A) (Table 2) (Dataset 2)**. The electron density at the binding interface is
356 unambiguous and included density for the entirety of the repeat region of the peptide **(Fig. S6).**
357 Looking at the binding interface between the two Fabs and peptide reveals the structural basis
358 for cross-reactivity **(Table 1) (Fig. S7) (Table S3)**. The paratope of B1E11K is highly enriched in
359 arginine and histidine residues giving rise to a highly electropositive groove **(Fig. 5B-5D)**. These
360 residues form a plethora of salt-bridging interactions with the glutamate residue side chains of
361 RESA repeats **(Fig. 5E)**. These interactions are supplemented by hydrogen bonding interactions
362 of backbone serine and glycine residues of the B1E11K paratope as well as a hydrogen bond
363 involving W33 found in the heavy chain of Fab B. Multiple hydrogen bonding interactions are
364 made with B1E11K through the side chains of the asparagine residues of RESA repeats (EENV)
365 **(Fig. 5F)** that would not exist in the context of binding to the repeats of Pf11.1 (EELV or EEVIP
366 or EEFIP or EEVVP) or Pfs230 (EEVG) **(Fig. 3C),** as these residues lack side chains that can
367 form hydrogen bonds. This likely leads to the observed higher specificity of B1E11K for RESA
368 repeats demonstrated in our ELISA experiments **(Fig. 3D)**.
369
370 Additionally, the crystal structure of the antibody-antigen complex revealed the presence of
371 homotypic antibody-antibody contacts, through two interfaces surrounding the repeat peptide
372 binding groove **(Fig. 5G) (Fig. S8) (Table S4)**. The first interface features a salt-bridging network
373 involving D60 of the Fab B kappa chain forming two salt bridges with R52 and H52A of the Fab A
374 HCDR2 **(Fig. 5H)**. Additionally, R54 of the Fab A HCDR2 forms two hydrogen bonds and a salt
375 bridge with the Fab B kappa chain side chains of S55 and E56. Finally, Y58 of the Fab B HCDR2
376 forms a hydrogen bond with the side chain of S53 of the Fab A HCDR2. The second interface is

377 less extensive featuring two hydrogen bonds between Y32 and S31 of the Fab B HCDR1 and the
378 Fab A KCDR1 T29 and R27, respectively **(Fig. 5I)**.
379
380 Analysis of the B1E11K sequences with IgBLAST (47) reveals that the B1E11K heavy and light
381 chain have high similarity to the IGHV3-7 and IGKV3-20 germline sequences **(Fig. S8)**. This
382 analysis also indicates multiple residues involved in the homotypic interaction interface have
383 undergone somatic hypermutation. Residues of the CDR2 heavy chain of Fab A, R52 and H52A,
384 and kappa chain CDR1 residues of Fab B, T29 and R27, form various electrostatic and van der
385 Waals interactions which are mutated from the inferred germline sequences **(Fig. 5F and 5G)**
386 **(Fig. S8-9)**. In summary, our biophysical and structural characterization revealed the basis of
387 cross-reactivity and specificity to RESA repeats (EENV) through a binding interface highly
388 electrostatic in nature, featuring affinity-matured homotypic interactions between adjacent
389 antibody molecules when in its antigen-bound state.
390
391
392 **Discussion:**
393
394 Here, we introduce an innovative strategy that circumvents the use of recombinant proteins, to
395 explore humoral immunity to *Pf* sexual proteins. We used target-agnostic MBC sorting and
396 activation, followed by screening to assess reactivity against *P. falciparum* gamete lysate and, for
397 a fraction of the sorted cells, gametocyte lysate. The approach enabled the identification of a
398 panel of mAbs targeting diverse *Pf* proteins, including some that exhibit transmission reducing
399 activity. The total number of isolated Abs was relatively low due to the limited number of cells
400 used. However, the identified B cells accounted for 5.6% of the total number, which suggest that
401 there is a relatively high proportion of B cells specific for gamete proteins in the memory
402 compartment of this donor, considering not all B cells were activated (typically 70-80 % activation
403 in our experiments). Furthermore, despite screening with a parasite extract containing a mixture
404 of intracellular and surface proteins, half of the mAbs displayed binding to the surface of gametes
405 , and/or exhibited TRA. This suggests antibody responses to surface proteins and proteins
406 involved in transmission were high in this particular donor, potentially explaining the potent TRA
407 observed with the serum.
408
409 Among the seven mAbs exhibiting TRA, three were found to recognize the well-defined TRA
410 targets Pfs48/45 and Pfs230. The B1C5L and B1C5K mAbs were shown to recognize Domain 2
411 of Pfs48/45 and exhibited moderate potency, as previously described for antibodies with such
412 specificity (27). These 2 mAbs were isolated from the same well and shared the same heavy
413 chain; their similar characteristics thus suggest that their binding is primarily mediated by the
414 heavy chain. Furthermore, a mAb identical to B1C5K was recently isolated from the same donor
415 using a single B cell selection approach with recombinant Pfs48/45 (27). The B2C10L mAb was
416 shown to recognize Pfs230 in gamete binding assays and western blot, but failed to bind the pro
417 and D1 domains of Pfs230 in ELISA. This confirms TRA may be mediated through binding to
418 domains other than pro-D1, the current main vaccine candidate (48), as previously observed for
419 rodent mAbs that were generated against native Pfs230 (49) (50) (51).
420
421 The remaining four mAbs exhibiting TRA did not clearly demonstrate recognition of either Pfs230
422 or Pfs48/45. Among those mAbs, B2E9L, and to a lesser extent B1C8L, showed recognition of
423 wildtype gametes but not gametes that lacked surface-bound Pfs230 and Pfs48/45. However,
424 Western blot did not identify any protein targeted by these two mAbs and they did not bind to
425 Pfs48/45 in ELISA. Therefore, we hypothesize these two mAbs target a protein associated with
426 the Pfs48/45-Pfs230 complex (52). An alternative explanation for the antigenicity of B2E9L and
427 B1C8L is that these two mAbs may target a Pfs230 conformational epitope that is not represented

428 in Western blot assays. The last two mAbs that exhibited TRA, B1D3L and B1F9K, displayed no
429 reactivity with the gamete surface, neither with wildtype nor gametes that lacked surface-bound
430 Pfs48/45 and Pfs230, and did not show any recognition in Western blot. In the case of B1D3L,
431 the selection during screening was based on recognition of the gametocyte lysate while testing
432 on the gamete extract was negative. This mAb may possibly target a protein only expressed on
433 gametocytes (indicating that the epitope might be conformational and not properly displayed in
434 Western blotting with gametocyte extract). Regarding B1F9K, it is somewhat surprising that this
435 mAb, which was originally selected based on positivity in the gamete extract ELISA, did not
436 display reactivity in SIFA while still exhibiting TRA. Further exploration is needed to understand
437 this apparent discrepancy. Overall, these latter mAbs, which do not recognize well-defined TRA
438 targets, demonstrated lower potency in the SMFA assay compared to some of the best
439 characterized mAbs with such activity. Nevertheless, they could still be of strong interest in
440 defining potential novel TRA targets, and further investigations are needed.
441
442 Seven of the fourteen mAbs isolated did not exhibit TRA. Of those, four exhibited some level of
443 binding to gamete surfaces: B1E11K, B2D10L, B1E7K and B2F7L (albeit very weakly). This may
444 suggest either the recognition of proteins involved in transmission but with an insufficient affinity
445 to exert a significant effect, recognition of non-functional epitopes in proteins that play a role in
446 transmission, or the recognition of proteins unrelated to the transmission process altogether.
447
448 B1E11K recognized various proteins from both the Pf sexual stage and asexual stages, all
449 containing glutamate-rich repeats. Repetitive regions rich in glutamate residues have been
450 previously found to be highly immunogenic in malaria-experienced individuals. A study
451 investigating antibody responses against asexual stage antigens of *Pf* associated with erythrocyte
452 invasion using sera from individuals from various cohorts found that the repetitive regions rich in
453 glutamate residues within these antigens were predominantly recognized (40). Another
454 investigation into sera from individuals from Uganda corroborated this finding (41). Raghavan et
455 al noted the antibodies that target these repeats may be potentially cross-reactive but emphasized
456 that such a claim could only be demonstrated by direct investigations into mAbs. To our
457 knowledge, only four mAbs that target glutamate-rich repeats have been described in which their
458 epitopes have been determined. Of those mAbs, three were obtained following mouse
459 immunization, and only one was of human origin. The murine mAbs 1A1 (53) and 1E10 (54)
460 recognize Pf11.1-derived repeat peptides ([PEE(L/V)VEEV(I/V)]$_2$); the murine mAb 9B11 (55) is
461 able to bind to a peptide containing four EENV repeats of RESA; and finally the human mAb 33G2
462 (56) is specific for a peptide repeat sequence found in Ag332 (VTEEI) (57). Despite all targeting
463 linear epitopes containing tandem glutamate residues (EE), only 33G2 appeared to exhibit cross-
464 reactivity (58) and none had been structurally characterized. Thus, our structure provides critical
465 insights into how glutamate-rich-repeat targeting antibodies from immune individuals can cross-
466 react with various *Pf* proteins expressed at different life cycle stages.
467
468 A most revealing observation from our structure is the presence of affinity-matured antibody-
469 antibody homotypic interactions in the context of recognizing repetitive tandem glutamate
470 residues present across the *Pf* proteome. The finding that B1E11K targets a repetitive epitope
471 whilst engaging in affinity-matured homotypic interactions is similar to how antibodies elicited
472 against repetitive elements of CSP can also bind through homotypic interactions (12) (14) (15)
473 (13) (16) (19) (59) (17) (18) (11). We have previously shown that B cells expressing B cell
474 receptors (BCRs) interacting via homotypic interactions activate more robustly in comparison to
475 B cells that have mutated BCRs that disrupt this interaction (12). This strong B cell activation,
476 presumably mediated through the cross-linking of multiple BCRs at the B cell surface (60), has
477 been suggested to limit affinity maturation in germinal centers, potentially due to early exit of B
478 cells, favouring the elicitation of short-term low-affinity antibodies to CSP over durable high-affinity

479 responses, thus leading to suboptimal protective responses (61). However, this phenomenon may
480 potentially be altered with the development of cross-reactive responses against repeats of slightly
481 different content (62) (63) (64). Whether such insights extend to other anti-repeats antibody
482 responses in general and anti-glutamate-rich repeats in particular remains largely unexplored.
483
484 Our observation of the recognition of RESA glutamate repeats by the B1E11K mAb through
485 homotypic interactions tends to confirm a generalizable property of B cell responses to repetitive
486 antigens where Abs can bind in close proximity. Here, we observed that B1E11K mAb exhibits a
487 fair degree of somatic hypermutation and a relatively high affinity for RESA and cross-reactivity
488 to other antigens. This finding provides further credence to the proposition that high affinity
489 matured Abs to repeats can be elicited when cross-reacting to motifs of slightly different content,
490 in the present case derived from antigens expressed at different stages of the *Pf* life cycle.
491 Nonetheless, cross-binding to repeats-sharing proteins from different stages, as demonstrated
492 with the B1E11K mAb, could also represent another mechanism by which repeated motifs may
493 impact protective responses. Indeed, antibodies elicited by one protein with repeats may hinder
494 subsequent potential protective responses to cross-recognized proteins expressed later in the
495 parasite life cycle through antibody feedback mechanisms such as epitope masking (41) (65) (66)
496 (67).
497
498 Ultimately, understanding the dynamics of how the immune system responds to repetitive
499 elements could be critical for the future rational design of malaria vaccines. A desired
500 characteristic for next-generation malaria vaccines will be the ability to elicit antibodies that can
501 inhibit at multiple stages of the parasite's life cycle to prevent infection, reduce clinical
502 manifestations, and lower the spread of the disease (68) (69). This could be accomplished by
503 designing a multi-stage malaria vaccine that displays antigens expressed at various points of the
504 parasite's life cycle. Utilizing glutamate-rich repeats in such a design may present benefits as a
505 single antigen could potentially give rise to sera which contain antibodies that can both lower the
506 clinical burden (asexual stage-targeting antibodies) and transmission of the disease (sexual
507 stage-targeting antibodies). Indeed, antibodies elicited against the repetitive elements described
508 here have been demonstrated to be associated with a lower incidence of disease (70) (71) (72)
509 as well as disrupt the maturation of sexual stage parasites (53) in *in vitro* assays – although we
510 note that mAb B1E11K isolated and characterized in this study did not show TRA.
511
512 As such, future work will be necessary to better understand the structure-activity relationships of
513 mAbs targeting *Pf* repetitive elements across life cycle stages, such as the glutamate-rich repeats,
514 and validate these targets as viable for next-generation malaria vaccines seeking the induction of
515 long-lived immunity. The high-throughput target-agnostic approach used here has a strong
516 potential for a further comprehensive exploration of humoral immunity to *Pf*.
517
518
519
520 **Material and methods:**
521
522 **PBMC sampling.**
523
524 (29)Donor A had lived in Central Africa for approximately 30 years and reported multiple malaria
525 infections during that period. At the time of sampling PBMCs, Donor A had recently returned to
526 the Netherlands and visited the hospital with a clinical malaria infection. After providing informed
527 consent, PBMCs were collected, but gametocyte prevalence and density were not recorded.
528
529 **Preparation of MBCs culture plates.**

530
531 Plates were prepared the day ahead of sorting and incubated at 37 °C. Three-hundred-eighty-
532 four-well cell culture plates (Corning #CLS3570-50EA) were prepared with the appropriate
533 memory B cell stimulation media one day before cell sorting, to allow the feeder cells
534 sedimentation at the bottom of the wells. Iscove's Modified Dulbecco's Medium (IMDM) (Gibco
535 #12440061) was complemented with 1% penicillin-streptomycin (Thermo Fisher Scientific
536 #10378016) and supplemented with 20% FBS (Gibco #16170-078). A cytokine cocktail was
537 added to stimulate MBCs activation, with IL21 (Preprotech #200-21) at 100 ng/ml and IL2
538 (Preprotech#200-02) at 51 ng/ml. Fibroblasts expressing CD40L "L cells" (73) were irradiated at
539 50 Gy and 5000 were added in each well as feeder cells.
540
541 **MBCs sorting.**
542
543 Cryopreserved PBMCs were thawed by a brief incubation in a 37 °C warm bath and stained with
544 the following Miltenyi REA antibodies before sorting by flow cytometry: anti-CD3 (#130-114-519),
545 anti-CD19 (#130-113-649), anti-CD20 (#130-113-649), anti-IgM (#130-113-476), anti-IgD (#130-
546 110-643) and anti-IgA (#130-113-476). An Aqua LIVE/DEAD stain was also used (Thermo Fisher
547 Scientific #L34957). Following staining, MBCs were sorted into the 384-well cell culture plates.
548 After an 11 day culture period, supernatants were harvested using a pipetting robot (Eppendorf
549 #5073) and transfered to storage plates (Greiner #788860-906). MBCs were lysed and their
550 mRNA purified using the mRNA TurboCapture kit for 384 wells (Qiagen #72271). Lysates were
551 stored at -80 °C. Lysates from selected wells were further transferred into 96-well RT-PCR plates
552 (Biorad #HSP9641) to perform RT-PCR.
553
554 **Gamete / gametocyte extract ELISA.**
555
556 Gamete or gametocyte lysate were prepared as described (27). Three hundred eighty four well
557 plates (Thermo Fisher Scientific #460372) were coated with 7500 lysed gametes / gametocytes
558 per well. Plates were incubated at 4°C overnight, then wells were washed three times with PBS-
559 Tween 0.05%, prior to 1 hour blocking (with a 1% BSA - 1% PBS-Tween 0.05% solution). Cell
560 culture supernatants (diluted ½ in blocking solution) were dispensed into the wells for a 1-hour
561 incubation step. Following washing, secondary antibody (Thermo Fisher Scientific #A18814)
562 diluted at 1/2000 was added and incubated for 1 h. Plates were then washed and 15 µl of CDP-
563 substrate (Thermo Fisher Scientific #T2146) was added. The reaction was measured using Biotek
564 Synergy 2 reader. Positivity threshold was determined as the average background OD + (3 x SD
565 (background OD)). 0.3 µg/mL TB31F (anti-Pfs48/45 mAb), and 1.0 µg/mL 2544 (anti-*Pf*s25 mAb)
566 were used as positive controls, while 30.0 µg/mL 399 (anti-CSP mAb) was used as negative
567 control.
568
569 **Monoclonal antibody isolation and production.**
570
571 Nested multiplexed PCRs were performed on single MBCs from selected wells following the
572 protocol outlined by Tiller et al (37). PCR products were sent for sequencing (Genewiz®) and
573 sequences analyzed for Ig gene features using the IMGT (ImMunoGeneTics) database (74). Ig
574 gene family-specific primers were used for cloning, as described by Tiller et al (PMID: 17996249)
575 (37). Purified PCR products were cloned into vectors encoding for either IgG1 lambda, kappa or
576 heavy constant regions. For transient mAb expression and secretion, HEK293 F cells were co-
577 transfected with plasmids coding the Ab heavy chain and the corresponding light chain using 293
578 Fectin (TF#12347500). A protein A-Sepharose column (Sigma #ge17-1279-03) was used for mAb
579 purification. Elution of mAbs was conducted with 4.5 ml of glycine 0.1 M (pH 2.5) and 500 µl of

580 Tris 1 M (pH 9). The purified mAbs were subsequently subjected to buffer exchange and
581 concentration with AmiconUltra (Merck #36100101).
582
583 **Fab production.**
584
585 The DNA sequences of VK and VH of the B1E11K Fab domain were cloned upstream of human
586 Igκ and Igγ1-CH1 domains respectively and inserted into a custom pcDNA3.4 expression vector.
587 The plasmids were co-transfected into FreeStyle 293 F cells that were cultured in FreeStyle 293
588 Expression Media (Gibco #12338018) using Fectopro (Polyplus, 101000003). The recombinant
589 Fab was purified via KappaSelect affinity chromatography (Cytiva #17545812) and cation
590 exchange chromatography (MonoS, Cytiva 17516801).
591
592 **Gamete surface immuno-fluorescence assay (SIFA).**
593
594 Gamete SIFA was performed with *Pf* NF54 wild-typeand Pfs48/45 knockout (75) strains. The
595 Pfs48/45 knockout lacks both surface-bound Pfs48/45 and Pfs230 (29) (35) (76)Wild-type or
596 Pfs48/45 KO gametes were obtained following gametocyte activation in FBS for 1 h at room
597 temperature. Gametes were washed with PBS and incubated with mAbs dilutions in PBS
598 containing 0.5% PBS and 0.05% NaN_3 (SIFA buffer) for 1 hr at 4 °C in sterile V bottom plates
599 (VWR#736-0223). After incubation, wells were washed three times with SIFA buffer and
600 secondary antibody Alexa Fluor® 488 Goat Anti-Mouse IgG (H+L) (Invitrogen#A11001) diluted
601 1/200 added for a 1-hour incubation step on ice. Following a washing step, gametes were
602 suspended in 4% paraformaldehyde and transferred into 384-well clear bottom black plates. Four
603 images per well were taken using the ImageXpress® Pico Cell Imaging System (Molecular
604 Devices).
605
606 **Western blot.**
607
608 For western blots with gametocyte extract, *Pf* NF54 gametocyte extract was prepared as
609 described above. The extract was mixed with NuPAGE™ LDS sample buffer (TF # NP0008) and
610 heated for 15 min at 56 °C. The equivalent of 1 million lysed gametocytes was deposited per lane.
611 A NuPAGE™ 4-12% Bis-Tris 2D-well gel (TF#NP0326BOX) was used for proteins separation.
612 Using the Trans-Blot Turbo system (Bio-Rad #1704150) samples were then transferred to a 0.22
613 µm nitrocellulose membrane (Bio-Rad #1620150). The blots were cut into strips, blocked with 5%
614 skimmed milk in PBS and incubated with 5 µg/ml of the mAb to be tested. Strips were incubated
615 with the secondary anti-human IgG-HRP antibody (Pierce#31412), diluted 1/5000 in PBS-T.
616 Clarity Western ECL substrate (Bio-Rad #1705060) was used for development and strips were
617 imaged with the ImageQuant LAS4000 equipment (GE Healthcare).
618 For western blot with recombinant proteins, we used Pfs230CMB (amino acids 444-730)
619 expressed in a plant-based transient expression system (77), and RESA3 (amino acids 570-
620 1090), RESA (amino acids 66-585), LSA3 (amino acids 805-1558) and Pf11.1 (amino acids 3657-
621 3734) that were expressed wheat germ cell free extract
622 (https://repository.ubn.ru.nl/bitstream/handle/2066/289602/289602.pdf?sequence=1). All
623 antigens contained a C-terminal His-tag. RESA and LSA3 also had an N-terminal GST-tag. The
624 equivalent of 150 ng of protein was loaded per lane. An SDS 4-20% gel (BioRad # 4561094) was
625 used for protein separation under non-reducing conditions. Further steps were performed
626 following the protocol described above.
627
628 **Recombinant Pfs48/45 and Pfs230 ELISA.**
629

630 ELISAs with full length Pfs48/45 and fragments thereof, and Pfs230CMB were performed as
631 previously described (27) (77). In short, Nunc MaxiSorp 96-wells plates (ThermoFisher) were
632 coated with 0.5 µg/mL recombinant Pfs48/45 or Pfs230CMB proteins, blocked with 5% skimmed
633 milk in PBS + 0.1% Tween-20 and washed. Plates were then incubated with 10 or 30 µg/mL mAb
634 in 1% skimmed milk in PBS. After washing, plates were incubated with 1:60,000 Goat anti-Human
635 IgG/HRP-conjugated antibody (Pierce, Cat. No. 31412) in 1% skimmed milk in PBS + 0.1%
636 Tween-20. After washing, plates were developed with 3,3′,5,5′-Tetramethylbenzidine (TMB) and
637 the reaction was stopped with H_2SO_4. Absorbance was measured at 450nm. mAbs were
638 considered positive when the absorbance was higher than the mean absorbance plus three
639 standard deviations of seven negative mAbs.
640
641 **MAb poly-reactivity testing in ELISA.**
642
643 The coating antigens were diluted to 1 µg/ml. Antigens used were: ssDNA (Sigma #D8899-5MG),
644 disialoganglioside GD1α (Sigma #G2392-1MG), lipopolysaccharide (Sigma #L2630-10MG),
645 transferrin (Sigma #T3309-100MG), apotransferrin (Sigma #T1147-100MG), hemocyanin (Sigma
646 #H7017-20MG), insulin (Sigma #I2643-25MG), cardiolipin (Sigma #C0563-10MG), albumin and
647 histone (Sigma #H9250-100MG). Secondary antibody used was a phosphatase-coupled goat
648 anti-human IgG (Jackson immuno #109 056 098). Optical densities were read at 405 nm, one
649 hour after the addition of pNPP.
650
651 **Standard Membrane Feeding Assay (SMFA).**
652
653 SMFA experiments were performed using *Pf* NF54 wild-type gametocytes with oocyst count
654 readout, following a protocol set up by Ponnudurai et al (78). Briefly, blood meals containing
655 cultured gametocytes mixed with antibodies were fed to *A. stephensi* mosquitoes (Nijmegen
656 colony). For each condition, 20 fully fed mosquitoes were analyzed. Reported antibody
657 concentrations are concentrations in the total blood meal volume. mAbs that showed >80%
658 transmission reducing activity (TRA), i.e. reduction in oocysts compared to a negative control,
659 were tested in a second independent SMFA experiment. Transmission reducing activity (TRA)
660 from one or two independent SMFA experiments was calculated using a negative binomial
661 regression model as previously described (79). SMFA data analyses were done in R (version
662 4.1.2).
663
664 **Microarray.**
665
666 Microarray design and protocol have been extensively detailed in (29) and (80) . Briefly, selection
667 proteins to be printed on the array was made on the basis of a systematic analyses of proteomic
668 data by Meerstein-Kessel et al (81). In total 943 protein targets representing 528 unique gene IDs
669 were expressed for the array using an in vitro transcription translation system; these were printed
670 onto nitrocellulose coated slides at the University of California, Irvine as described previously (80).
671 Microarray slides were rehydrated in blocking buffer (GVS #10485356) while B1E11K was diluted
672 1:100 in a 20% E. coli lysate/blocking buffer solution and incubated for 30 min. Blocking buffer
673 was discarded and diluted B1E11K added to the array slides for incubation overnight at 4° C with
674 continual rocking. Following three washes with TBS-Tween-20 0.05%, slides were probed with a
675 fluorophore conjugated secondary antibody (Southern Biotech, Goat Anti-Human IgG-TXRD) at
676 a concentration of 0.5 µg/mL (1:2000) in 2% E. coli lysate/blocking buffer solution. After three
677 washes, slides were removed from their casettes and rinsed in ddH20air dried in a centrifuge and
678 scanned using a GenePix 4300A High-resolution Microarray Scanner (Molecular Devices). Data
679 treatment and analysis were performed using R (82). Correction for local array target spot
680 background was done using the 'backgroundCorrect' function of the limma package (83).

681 Background corrected values were log2 transformed and normalised to systematic effects by
682 subtraction of the median signal intensity of the negative IVTT controls (internally within four
683 subarrays per sample). The final normalised data are a log2 MFI ratio of target to control reactivity:
684 a value of 0 represents equality with the vehicle control, and a value of 1 indicates a signal twice
685 as high.
686
687 **Immunoprecipitation.**
688
689 Briefly, we used tosyl-activated beads (Invitrogen #14203) to covalently link B1E11K and
690 incubated these beads with a gametocyte lysate to enable antigen capture. Immunoprecipitated
691 antigens were eluted, and the elution fraction was run on an SDS-PAGE gel and silver-stained. A
692 negative control immunoprecipitation experiment was performed using an anti-HIV gp120 mAb.
693 As shown in **sup Fig 2B**, two bands with a molecular weight greater than 250 kDa, and a third
694 one with a molecular weight around 55 kDa were specifically detected in the B1E11K
695 immunoprecipitate, in comparison to the control antibody. The 3 bands were cut and sent for mass
696 spectrometry analysis. Data were analyzed by querying the entire proteome of *Plasmodium*
697 *falciparum* (NF54 isolate) in the Uniprot database.
698
699 **Peptide synthesis.**
700
701 Peptides were produced by P. Verdié team, IBMM - SynBio3, Montpellier, France. Lyophilized
702 peptides were solubilized in PBS.
703
704 **ELISA with biotinylated peptides.**
705
706 ELISA protocol was similar to the protocol described above. Briefly, 96-well ELISA plates were
707 coated overnight at 4° C with 0.5 µg/ml of streptavidin (TF # 434301). Plates were washed and
708 then blocked for 1 h. Following wash, peptides diluted at 0.5 µg/ml were added to the plates for a
709 1 h incubation. The plates were washed and serially diluted mAbs were added. mAb fixation was
710 detected using phosphatase-coupled goat anti-human IgG (Jackson Immuno #109 056 098) and
711 para-nitrophenylphosphate (Interchim #UP 664791). The enzymatic reaction was measured at
712 405 nm using a TECAN Spark 10M plate reader. Half maximal effective concentration (EC50)
713 was calculated from raw data (O.D) after normalization using GraphPad Prism (version 9) "log
714 agonist versus normalized response" function.
715
716 **BioLayer Interferometry (BLI) assay.**
717
718 All BLI experiments were performed using an Octet Red96e Instrument (PallForteBio), at 25°C
719 and under 1000 rpm agitation. SAX biosensors (Sartorius # 18-5117) were pre-wetted in BLI
720 Buffer [PBS (pH 7.4) + 0.01% (w/v) BSA + 0.002% (v/v) Tween-20] for 10 min. Biotinylated
721 peptides were loaded onto the biosensors until the top concentration of B1E11K Fab utilized in
722 kinetic assays (2500 nM for RESA 10 AA peptide and 625 nM for RESA P2 peptide) yielded a
723 response value of ~ 1.2 nm. An association step was conducted by dipping the sensors into a
724 titration series of ½ serially diluted B1E11K Fab for 30 seconds. The dissociation step was
725 conducted by dipping the biosensors into BLI Buffer for 1200 seconds. Background subtractions
726 were done using measurements where experiments were performed with biosensors treated in
727 the same conditions but replacing Fab solution with BLI Buffer. Kinetic data were processed using
728 the manufacturer's software (Data analysis HT v11.1).
729
730 **Isothermal Titration Calorimetry.**
731

732 An Auto-ITC200 (Malvern) was used to conduct calorimetric experiments. The RESA P2 peptide,
733 RESA 10AA peptide, and recombinant B1E11K Fab were buffer-exchanged into Tris-buffered
734 saline (20 mM Tris pH 7.0, and 150 mM NaCl). The B1E11K Fab was concentrated at 90 - 110
735 μM for experiments utilizing the RESA P2 peptide and 60 - 70 μM for those utilizing the RESA
736 10AA peptide. The RESA P2 peptide and RESA 10AA peptide were concentrated at 5-6 μM and
737 7-10 μM respectively. Fab (syringe) was titrated into the cell (peptide) at 25°C using a protocol
738 involving 19 injections each at a volume of 2.0 μL. The curves were fitted to a 2:1 or 1:1 binding
739 model using the MicroCal ITC Origin 7.0 Analysis Software.
740
741 **Size-Exclusion Chromatography-Multi-Angle Light Scattering (SEC-MALS).**
742
743 SEC-MALS experiments were performed at 4°C using a Superdex 200 Increase 10/300 GL
744 (Cytiva #GE17-5175-01) column. RESA P2 peptide was incubated with B1E11K Fab at a 1:6
745 molar ratio for 30 minutes prior to loading onto the Superdex 200 column. The column was set up
746 onto an Agilent Technologies 1260 Infinity II HPLC coupled with a MiniDawn Treos MALS detector
747 (Wyatt), Quasielastic light scattering (QELS) detector (Wyatt), and Optilab T-reX refractive index
748 (RI) detector (Wyatt). Data processing was performed using the ASTRA software (Wyatt).
749
750 **Negative Stain Electron Microscopy (nsEM) and Image Processing.**
751
752 Fractions of the first peak of the SEC-MALS experiments containing the 2:1 B1E11K:RESA P2
753 complex were used to make nsEM grids. 50 μg/mL of the complex was deposited onto homemade
754 carbon film-coated grids (previously glow-discharged in air for 15s) and stained with 2% uranyl
755 formate. Data was collected onto a Hitachi HT7800 microscope paired with an EMSIS Xarosa 20
756 Megapixel CMOS camera. Micrographs were taken with the microscope operating at 120 kV at
757 80,000x magnification with a pixel size of 1.83 Å/px. Image processing, particle picking,
758 extractions, 2D classifications, and 3D reconstructions were done in cryoSPARC v2 (84).
759
760 **X-Ray Crystallography and Structural Determination.**
761
762 The RESA P2 peptide was incubated with B1E11K Fab at a 1:5 molar ratio for 30 minutes prior
763 to loading onto a Superdex 200 column Increase 10/300 GL column. Fractions containing the
764 complex were pooled and concentrated at 8.6 mg/mL. A seed stock prepared from a previous
765 crystallization trial was used for seeding. The stock was prepared from condition G9 of a JCSG
766 Top96 screen (0.2M (NH4)2SO4 25% [w/v] PEG4000, and 0.1M sodium acetate [pH 4.6]). The
767 complex, reservoir solution, and seed stock were mixed at a 3:4:1 volumetric ratio into an
768 optimization tray derived from condition G9 of the JCSG Top96 screen. Crystals grew within 6
769 hours in a reservoir condition consisting of (0.1M NH4)2SO4 25% (w/v) PEG4000, and 0.1M
770 sodium acetate (pH 5.2). Crystals were cryo-protected with 15% ethylene glycol (v/v) before being
771 flash-frozen in liquid nitrogen. Data collection was performed at the 23-ID-B beamline at the
772 Argonne National Laboratory Advanced Photon Source. Datasets were initially processed using
773 autoproc (85) and further optimized using xdsgui (86). Molecular replacement was performed
774 using PhaserMR (87) followed by multiple rounds of refinement using phenix.refine (88) and Coot
775 (89). Inter- and intra-molecular contacts were determined using PISA (90) and manual inspection.
776 Structural figures were generated using UCSF ChimeraX (91) (92).
777
778 **Acknowledgements:**
779
780 We thank A. Guarino for her support to antibody production, N. Thielens for her input during the
781 course of this work, Y. Couté for the proteomics analysis, J-B. Reiser for the preliminary BLI
782 experiments, L. Chaperot for providing CD40L expressing fibroblasts, E. Thai and D. Ivanochko

783 for their contributions to X-ray data collection and structure determination, K. Teelen for
784 assistance with ELISAs, M. van de Vegte-Bolmer and R. Stoter for parasite culture, G.J. van
785 Gemert and L. Pelser and A. Pouwelsen and J. Kuhnen and J. Klaassen and S. Mulder for
786 mosquito rearing and dissection, and K. Koolen for support with ELISA and gamete binding
787 experiments. Furthermore, we would like to thank Jessica Chichester (Fraunhofer) for providing
788 Pfs230CMB. This work was supported in part by the Bill & Melinda Gates Foundation
789 (OPP1108403). This work was also undertaken, in part, thanks to funding from the Canadian
790 Institutes for Health Research and was supported by the CIFAR Azrieli Global Scholar program
791 (JPJ), the Ontario Early Researcher Award program (JPJ), and the Canada Research Chair
792 program (JPJ). RY was supported by a Canada Graduate Scholarship - Master's (CGS-M). WS
793 is supported by a Wellcome Trust Fellowship (218676/Z/19/Z). MMJ is supported by a Vidi grant
794 from the Netherlands Organisation for Scientific Research (Vidi fellowship number 192.061). The
795 proteomic experiments were partially supported by ANR grant ProFI (Proteomics French
796 Infrastructure, ANR-10-INBS-08) and GRAL, a program from the Chemistry Biology Health (CBH)
797 Graduate School of University Grenoble Alpes (ANR-17-EURE-0003). This work used the
798 platforms of the Grenoble Instruct-ERIC center (ISBG ; UAR 3518 CNRS-CEA-UGA-EMBL) within
799 the Grenoble Partnership for Structural Biology (PSB), supported by FRISBI (ANR-10-INBS-
800 0005-02) and GRAL, financed within the University Grenoble Alpes graduate school (Ecoles
801 Universitaires de Recherche) CBH-EUR-GS (ANR-17-EURE-0003). Molecular graphics were
802 generated using UCSF ChimeraX, developed by the Resource for Biocomputing, Visualization,
803 and Informatics (University of California, San Francisco) with support from the National Institutes
804 of Health (R01-GM129325) and the Office of Cyber Infrastructure and Computational Biology,
805 National Institute of Allergy and Infectious Diseases.The BLI, ITC and SEC-MALS instruments
806 were accessed at the Structural and Biophysical Core Facility, The Hospital for Sick Children, and
807 EM data was collected at the Nanoscale Biomedical Imaging Facility, The Hospital for Sick
808 Children, supported by the Canada Foundation for Innovation and Ontario Research Fund. X-ray
809 diffraction experiments were in part performed using beamlines 23-ID-B at GM/CA@APS, which
810 has been funded by the National Cancer Institute (ACB-12002) and the National Institute of
811 General Medical Sciences (AGM-12006, P30GM138396). This research used resources of the
812 Advanced Photon Source, a U.S. Department of Energy (DOE) Office of Science User Facility
813 operated for the DOE Office of Science by Argonne National Laboratory under Contract No. DE-
814 AC02-06CH11357. The Eiger 16M detector at GM/CA-XSD was funded NIH grant S10
815 OD012289. X-ray diffraction experiments were also performed using beamline AMX-17-ID-1 at
816 the National Synchrotron Light Source II, a U.S. Department of Energy (DOE) Office of Science
817 User Facility operated for the DOE Office of Science by Brookhaven National Laboratory under
818 Contract No. DE-SC0012704. The Center for BioMolecular Structure (CBMS) is primarily
819 supported by the National Institutes of Health, National Institute of General Medical Sciences
820 (NIGMS) through a Center Core P30 Grant (P30GM133893), and by the DOE Office of Biological
821 and Environmental Research (KP1607011). X-ray diffraction experiments were also performed
822 using beamline CMCF-ID at the Canadian Light Source, a national research facility of the
823 University of Saskatchewan, which is supported by the Canada Foundation for Innovation (CFI),
824 the Natural Sciences and Engineering Research Council (NSERC), the National Research
825 Council (NRC), the Canadian Institutes of Health Research (CIHR), the Government of
826 Saskatchewan, and the University of Saskatchewan.

827 **References:**
828

829 1. World malaria report 2021.
830 2. Wicht KJ, Mok S, Fidock DA. Molecular Mechanisms of Drug Resistance in
831 Plasmodium falciparum Malaria. Vol. 74, Annual Review of Microbiology.
832 Annual Reviews Inc.; 2020. p. 431–54.
833 3. Florens L, Washburn MP, Dale Raine J, Anthony RM, Graingerk M, David
834 Haynes J, et al. A proteomic view of the Plasmodium falciparum life cycle
835 [Internet]. 2002. Available from: www.nature.com/nature
836 4. Cowman AF, Healer J, Marapana D, Marsh K. Malaria: Biology and
837 Disease. Cell [Internet]. 2016;167(3):610–24. Available from:
838 http://dx.doi.org/10.1016/j.cell.2016.07.055
839 5. Rosenberg R. Malaria: some considerations regarding parasite productivity.
840 Trends Parasitol. 2008 Nov;24(11):487–91.
841 6. Laurens MB. RTS,S/AS01 vaccine (Mosquirix^{TM}): an overview. Hum
842 Vaccin Immunother. 2019;
843 7. Datoo MS, Dicko A, Tinto H, Ouédraogo JB, Olotu A, Beaumont E, et al. A
844 phase III randomised controlled trial evaluating the malaria vaccine
845 candidate R21/Matrix-M^{TM} in African children [Internet]. Available from:
846 https://ssrn.com/abstract=4584076
847 8. Cerami C, Frevert U, Sinnis P, Takacs B, Clavijo P, Santos MJ, et al. The
848 Basolateral Domain of the Hepatocyte Plasma Membrane Bears Receptors
849 for the Circumsporozoite Protein of Plasmodium falciparum Sporozoites.
850 Vol. 70, Cell. 1992.
851 9. Frevert U, Sinnis P, Cerami C, Shrefl W, Takacs B, Nussenzweig V. Malaria
852 Circumsporozoite Protein Binds to Heparan Sulfate Proteoglycans
853 Associated with the Surface Membrane of Hepatocytes [Internet]. Available
854 from: http://rupress.org/jem/article-pdf/177/5/1287/1674538/1287.pdf
855 10. Ménard Robert, Sultan Ali, Cortes Claudio, Altszuler Rita, van Dijk Mélissa,
856 Janse Chris, et al. Circumsporozoite protein is required for development of
857 malaria sporozoites in mosquitoes.
858 11. Kucharska I, Thai E, Srivastava A, Rubinstein JL, Pomès R, Julien JP.
859 Structural ordering of the plasmodium berghei circumsporozoite protein
860 repeats by inhibitory antibody 3d11. Elife. 2020 Oct 1;9:1–25.
861 12. Imkeller K, Scally SW, Bosch A, Martí GP, Costa G, Triller G, et al.
862 Antihomotypic affinity maturation improves human B cell responses against
863 a repetitive epitope [Internet]. Available from: www.imgt.org/genedb/.
864 13. Martin GM, Torres JL, Pholcharee T, Oyen D, Flores-Garcia Y, Gibson G, et
865 al. Affinity-matured homotypic interactions induce spectrum of PfCSP
866 structures that influence protection from malaria infection. Nat Commun.
867 2023 Dec 1;14(1).
868 14. Pholcharee T, Oyen D, Flores-Garcia Y, Gonzalez-Paez G, Han Z, Williams
869 KL, et al. Structural and biophysical correlation of anti-NANP antibodies
870 with in vivo protection against P. falciparum. Nat Commun. 2021 Dec
871 1;12(1).
872 15. Oyen D, Torres JL, Cottrell CA, Richter King C, Wilson IA, Ward AB.
873 Cryo-EM structure of P. falciparum circumsporozoite protein with a vaccine-

elicited antibody is stabilized by somatically mutated inter-Fab contacts. Vol. 4, Sci. Adv. 2018.

16. Martin GM, Fernández-Quintero ML, Lee WH, Pholcharee T, Eshun-Wilson L, Liedl KR, et al. Structural basis of epitope selectivity and potent protection from malaria by PfCSP antibody L9. Nat Commun. 2023 Dec 1;14(1).
17. Kucharska I, Hossain L, Ivanochko D, Yang Q, Rubinstein JL, Pomès R, et al. Structural basis of Plasmodium vivax inhibition by antibodies binding to the circumsporozoite protein repeats. Elife. 2022 Jan 1;11.
18. Murugan R, Scally SW, Costa G, Mustafa G, Thai E, Decker T, et al. Evolution of protective human antibodies against Plasmodium falciparum circumsporozoite protein repeat motifs. Nature Medicine 2020 26:7 [Internet]. 2020 May 25 [cited 2023 Oct 22];26(7):1135–45. Available from: https://www.nature.com/articles/s41591-020-0881-9
19. Tripathi P, Bender MF, Lei H, Da Silva Pereira L, Shen CH, Bonilla B, et al. Cryo-EM structures of anti-malarial antibody L9 with circumsporozoite protein reveal trimeric L9 association and complete 27-residue epitope. Structure [Internet]. 2023 Apr 6 [cited 2023 Oct 22];31(4):480-491.e4. Available from: http://www.cell.com/article/S0969212623000436/fulltext
20. Efficacy and safety of RTS,S/AS01 malaria vaccine with or without a booster dose in infants and children in Africa: Final results of a phase 3, individually randomised, controlled trial. The Lancet. 2015 Jul 4;386(9988):31–45.
21. Wadman M. First malaria vaccine slashes childhood deaths. Science (1979) [Internet]. 2023 Oct 27;382(6669):357–357. Available from: https://www.science.org/doi/10.1126/science.adl5521
22. Golumbeanu M, Yang GJ, Camponovo F, Stuckey EM, Hamon N, Mondy M, et al. Leveraging mathematical models of disease dynamics and machine learning to improve development of novel malaria interventions. Infect Dis Poverty. 2022 Dec 1;11(1).
23. Stone WJR, Dantzler KW, Nilsson SK, Drakeley CJ, Marti M, Bousema T, et al. Naturally acquired immunity to sexual stage P. Falciparum parasites. Vol. 143, Parasitology. Cambridge University Press; 2016. p. 187–98.
24. Duffy PE. Transmission-Blocking Vaccines: Harnessing Herd Immunity for Malaria Elimination. Vol. 20, Expert Review of Vaccines. Taylor and Francis Ltd.; 2021. p. 185–98.
25. Roeffen W, Teelen K, Van As J, Vd Vegte-Bolmer M, Eling W, Sauerwein R. Plasmodium falciparum: Production and characterization of rat monoclonal antibodies specific for the sexual-stage Pfs48/45 antigen. Exp Parasitol. 2001;97(1):45–9.
26. Ivanochko D, Fabra-García A, Teelen K, van de Vegte-Bolmer M, van Gemert GJ, Newton J, et al. Potent transmission-blocking monoclonal antibodies from naturally exposed individuals target a conserved epitope on Plasmodium falciparum Pfs230. Immunity. 2023 Feb 14;56(2):420-432.e7.
27. Fabra-García A, Hailemariam S, de Jong RM, Janssen K, Teelen K, van de Vegte-Bolmer M, et al. Highly potent, naturally acquired human monoclonal

920 antibodies against Pfs48/45 block Plasmodium falciparum transmission to
921 mosquitoes. Immunity. 2023 Feb 14;56(2):406-419.e7.
922 28. Kundu P, Semesi A, Jore MM, Morin MJ, Price VL, Liang A, et al.
923 Structural delineation of potent transmission-blocking epitope I on malaria
924 antigen Pfs48/45. Nat Commun. 2018 Dec 1;9(1).
925 29. Stone WJR, Campo JJ, Ouédraogo AL, Meerstein-Kessel L, Morlais I, Da D,
926 et al. Unravelling the immune signature of Plasmodium falciparum
927 transmission-reducing immunity. Nat Commun. 2018 Dec 1;9(1).
928 30. Coelho CH, Tang WK, Burkhardt M, Galson JD, Muratova O, Salinas ND,
929 et al. A human monoclonal antibody blocks malaria transmission and defines
930 a highly conserved neutralizing epitope on gametes. Nat Commun. 2021 Dec
931 1;12(1).
932 31. Tang WK, Coelho CH, Miura K, Nguemwo Tentokam BC, Salinas ND,
933 Narum DL, et al. A human antibody epitope map of Pfs230D1 derived from
934 analysis of individuals vaccinated with a malaria transmission-blocking
935 vaccine. Immunity. 2023 Feb 14;56(2):433-443.e5.
936 32. Ko KT, Lennartz F, Mekhaiel D, Guloglu B, Marini A, Deuker DJ, et al.
937 Structure of the malaria vaccine candidate Pfs48/45 and its recognition by
938 transmission blocking antibodies. Nat Commun. 2022 Dec 1;13(1).
939 33. Lennartz F, Brod F, Dabbs R, Miura K, Mekhaiel D, Marini A, et al.
940 Structural basis for recognition of the malaria vaccine candidate Pfs48/45 by
941 a transmission blocking antibody. Nat Commun. 2018 Dec 1;9(1).
942 34. Singh K, Burkhardt M, Nakuchima S, Herrera R, Muratova O, Gittis AG, et
943 al. Structure and function of a malaria transmission blocking vaccine
944 targeting Pfs230 and Pfs230-Pfs48/45 proteins. Commun Biol. 2020 Dec
945 1;3(1).
946 35. Eksi S, Czesny B, Van Gemert GJ, Sauerwein RW, Eling W, Williamson
947 KC. Malaria transmission-blocking antigen, Pfs230, mediates human red
948 blood cell binding to exflagellating male parasites and oocyst production.
949 Mol Microbiol. 2006 Aug;61(4):991–8.
950 36. Brooks SR, Williamson KC. Proteolysis of Plasmodium falciparum surface
951 antigen, Pfs230, during gametogenesis [Internet]. Vol. 106, Molecular and
952 Biochemical Parasitology. 2000. Available from:
953 www.elsevier.com/locate/parasitology
954 37. Tiller T, Meffre E, Yurasov S, Tsuiji M, Nussenzweig MC, Wardemann H.
955 Efficient generation of monoclonal antibodies from single human B cells by
956 single cell RT-PCR and expression vector cloning. J Immunol Methods.
957 2008 Jan 1;329(1–2):112–24.
958 38. Kundu P, Semesi A, Jore MM, Morin MJ, Price VL, Liang A, et al.
959 Structural delineation of potent transmission-blocking epitope I on malaria
960 antigen Pfs48/45. Nat Commun [Internet]. 2018 Dec 26 [cited 2019 Jan
961 14];9(1):4458. Available from: http://www.nature.com/articles/s41467-018-
962 06742-9
963 39. Coelho CH, Tang WK, Burkhardt M, Galson JD, Muratova O, Salinas ND,
964 et al. A human monoclonal antibody blocks malaria transmission and defines

965 a highly conserved neutralizing epitope on gametes. Nat Commun [Internet].
966 2021;1–12. Available from: http://dx.doi.org/10.1038/s41467-021-21955-1
967 40. Hou N, Jiang N, Ma Y, Zou Y, Piao X, Liu S, et al. Low-Complexity
968 Repetitive Epitopes of Plasmodium falciparum Are Decoys for Humoural
969 Immune Responses. Front Immunol. 2020 Apr 15;11.
970 41. Raghavan M, Kalantar KL, Duarte E, Teyssier N, Takahashi S, Kung AF, et
971 al. Proteome-wide antigenic profiling in Ugandan cohorts identifies
972 associations between age, exposure intensity, and responses to repeat-
973 containing antigens in Plasmodium falciparum. Elife. 2023 Feb 1;12.
974 42. Cardoso RMF, Zwick MB, Stanfield RL, Kunert R, Binley JM, Katinger H,
975 et al. Broadly neutralizing anti-HIV antibody 4E10 recognizes a helical
976 conformation of a highly conserved fusion-associated motif in gp41.
977 Immunity. 2005;22(2):163–73.
978 43. Heger A, Holm L. Rapid Automatic Detection and Alignment of Repeats in
979 Protein Sequences. 2000.
980 44. Williamsona· KC, Fujiokab H, Aikawab M, Kaslowc DC. Stage-specific
981 processing of Pfs230, a Plasmodium falciparum transmission-blocking
982 vaccine candidate. Vol. 78, Molecular and Biochemical Parasitology. 1996.
983 45. De Jong RM. Towards efficacious transmission blocking malaria vaccines
984 The long and winding path.. Towards efficacious transmission blocking
985 malaria vaccines. 2023.
986 46. Kratochvil S, Shen CH, Lin YC, Xu K, Nair U, Da Silva Pereira L, et al.
987 Vaccination in a humanized mouse model elicits highly protective PfCSP-
988 targeting anti-malarial antibodies. Immunity. 2021 Dec 14;54(12):2859-
989 2876.e7.
990 47. Ye J, Ma N, Madden TL, Ostell JM. IgBLAST: an immunoglobulin variable
991 domain sequence analysis tool. Nucleic Acids Res. 2013;41(Web Server
992 issue).
993 48. Miura K, Takashima E, Pham TP, Deng B, Zhou L, Huang WC, et al.
994 Elucidating functional epitopes within the N-terminal region of malaria
995 transmission blocking vaccine antigen Pfs230. NPJ Vaccines. 2022 Dec
996 1;7(1).
997 49. Simons LM, Ferrer P, Gombakomba N, Underwood K, Herrera R, Narum
998 DL, et al. Extending the range of Plasmodium falciparum transmission
999 blocking antibodies. Vaccine. 2023 May 16;41(21):3367–79.
1000 50. Inklaar MR, de Jong RM, Bekkering ET, Nagaoka H, Fennemann FL, Teelen
1001 K, et al. Pfs230 Domain 7 is targeted by a potent malaria transmission-
1002 blocking monoclonal antibody. NPJ Vaccines. 2023 Dec 1;8(1).
1003 51. de Jong RM, Meerstein-Kessel L, Da DF, Nsango S, Challenger JD, van de
1004 Vegte-Bolmer M, et al. Monoclonal antibodies block transmission of
1005 genetically diverse Plasmodium falciparum strains to mosquitoes. Vol. 6, npj
1006 Vaccines. Nature Research; 2021.
1007 52. Simon N, Kuehn A, Williamson KC, Pradel G. Adhesion protein complexes
1008 of malaria gametocytes assemble following parasite transmission to the
1009 mosquito. Parasitol Int. 2016 Feb 1;65(1):27–30.

1010 53. Feng Z, Hoffmann KN, Nussenzweig RS, Tsuji M, Fujioka H, Aikawa M, et
1011 al. Pfs2400 Can Mediate Antibody-dependent Malaria Transmission
1012 Inhibition and May Be the Plasmodium Falciparum 11.1 Gene Product
1013 [Internet]. Available from: http://rupress.org/jem/article-
1014 pdf/177/2/273/1103419/273.pdf
1015 54. Scherf A, Carter' R, Petersen2 C, Alano3 P, Nelson2 R, Aikawa4 M, et al.
1016 Gene inactivation of Pf 11-1 of Plasmodium falciparum by chromosome
1017 breakage and healing: identification of a gametocyte-specific protein with a
1018 potential role in gametogenesis. Vol. 1, The EMBO Journal. 1992.
1019 55. Masuda A, Zavala F, Nussenzweig V, Nussenzweig RS. Monoclonal anti-
1020 gametocyte antibodies identify an antigen present in all blood stages of
1021 Plasmodium faIciparum. Vol. 19, Molecular and Biochemical Parasitology.
1022 1986.
1023 56. Udomsangpetch Rachanee, Lundgren Katarina, Berzins Klaus, Wahlin
1024 Birgitta, Perlmann Hedvig, Troye-Blomberg Marita, et al. Human
1025 monoclonal antibodies to Pf 155 a major antigen of malaria parasite
1026 Plasmodium falciparum.
1027 57. Ahlborg N, Berzins K, Perlmann P. Definition of the epitope recognized by
1028 the Plasmodiumfalciparum-reactive human monoclonal antibody 33G2. Vol.
1029 46, Molecular and Biochemical Parasitology. 1991.
1030 58. Udomsangpetch Rachanee, Carlsson Jan, Wahlin Birgitta, Holmquist Goran,
1031 Ozaki Luiz, Scherf Arthur, et al. Reactivity of the human monoclonal
1032 antibody 33G2 with repeated sequences of three distinct Plasmodium
1033 falciparum antigens [Internet]. 2018. Available from:
1034 http://www.jimmunol.org/content/142/10/3620
1035 59. Kucharska I, Binter Š, Murugan R, Scally SW, Ludwig J, Prieto K, et al.
1036 High-density binding to Plasmodium falciparum circumsporozoite protein
1037 repeats by inhibitory antibody elicited in mouse with human
1038 immunoglobulin repertoire. PLoS Pathog. 2022 Nov 1;18(11).
1039 60. Clutterbuck EA, Lazarus R, Yu LM, Bowman J, Bateman EAL, Diggle L, et
1040 al. Pneumococcal conjugate and plain polysaccharide vaccines have
1041 divergent effects on antigen-specific B cells. Journal of Infectious Diseases.
1042 2012 May 1;205(9):1408–16.
1043 61. Wahl I, Wardemann H. How to induce protective humoral immunity against
1044 Plasmodium falciparum circumsporozoite protein. Vol. 219, Journal of
1045 Experimental Medicine. Rockefeller University Press; 2022.
1046 62. Murugan R, Scally SW, Costa G, Mustafa G, Thai E, Decker T, et al.
1047 Evolution of protective human antibodies against Plasmodium falciparum
1048 circumsporozoite protein repeat motifs. Nat Med. 2020 Jul 1;26(7):1135–45.
1049 63. Ludwig J, Scally SW, Costa G, Hoffmann S, Murugan R, Lossin J, et al.
1050 Glycosylated nanoparticle-based PfCSP vaccine confers long-lasting
1051 antibody responses and sterile protection in mouse malaria model. NPJ
1052 Vaccines. 2023 Dec 1;8(1).
1053 64. Thai E, Murugan R, Binter Š, Burn Aschner C, Prieto K, Kassardjian A, et
1054 al. Molecular determinants of cross-reactivity and potency by VH3-33
1055 antibodies against the Plasmodium falciparum circumsporozoite protein. Cell

Rep [Internet]. 2023 Nov;42(11):113330. Available from: https://linkinghub.elsevier.com/retrieve/pii/S2211124723013426

65. Chatterjee D, Lewis FJ, Sutton HJ, Kaczmarski JA, Gao X, Cai Y, et al. Avid binding by B cells to the Plasmodium circumsporozoite protein repeat suppresses responses to protective subdominant epitopes. Cell Rep. 2021 Apr 13;35(2).

66. Chatterjee D, Cockburn IA. The challenges of a circumsporozoite protein-based malaria vaccine. Expert Rev Vaccines [Internet]. 2021 Feb 1 [cited 2023 Oct 30];20(2):113–25. Available from: https://www.tandfonline.com/doi/abs/10.1080/14760584.2021.1874924

67. McNamara HA, Idris AH, Sutton HJ, Vistein R, Flynn BJ, Cai Y, et al. Antibody Feedback Limits the Expansion of B Cell Responses to Malaria Vaccination but Drives Diversification of the Humoral Response. Cell Host Microbe. 2020 Oct 7;28(4):572-585.e7.

68. Nahrendorf W, Scholzen A, Sauerwein RW, Langhorne J. Cross-stage immunity for malaria vaccine development. Vaccine. 2015 Dec 22;33(52):7513–7.

69. Julien JP, Wardemann H. Antibodies against Plasmodium falciparum malaria at the molecular level. Vol. 19, Nature Reviews Immunology. Nature Research; 2019. p. 761–75.

70. Riley EM, Allen SJ, Troye-Blomberg M, Bennett S, Perlmann H, Andersson G, et al. Association between immune recognition of the malaria vaccine candidate antigen Pf155/RESA and resistance to clinical disease: a prospective study in a malaria-endemic region of West Africa. Trans R Soc Trop Med Hyg [Internet]. 1991 Jul 1 [cited 2023 Oct 22];85(4):436–43. Available from: https://dx.doi.org/10.1016/0035-9203(91)90207-F

71. Petersen E, Høgh B, Marbiah NT, Perlmann H, Willcox M, Dolopaie E, et al. A longitudinal study of antibodies to the Plasmodium falciparum antigen Pf155/RESA and immunity to malaria infection in adult Liberians. Trans R Soc Trop Med Hyg [Internet]. 1990 Jun 1 [cited 2023 Oct 22];84(3):339–45. Available from: https://dx.doi.org/10.1016/0035-9203(90)90307-Z

72. Berzins K, Perlmann H, Wahlin B, Ekre HP, Hogh B, Petersen E, et al. Passive Immunization of Aotus Monkeys with Human Antibodies to the Plasmodium falciparum Antigen Pfl55/RESA [Internet]. Vol. 59, INFECTION AND IMMUNITY. 1991. Available from: https://journals.asm.org/journal/iai

73. Garrone P, Neidhardt EM, Garcia E, Galibert L, Van Kooten C, Banchereau J. Fas Ligation Induces Apoptosis of CD40-activated Human B Lymphocytes.

74. Lefranc MP, Giudicelli V, Duroux P, Jabado-Michaloud J, Folch G, Aouinti S, et al. IMGT R, the international ImMunoGeneTics information system R 25 years on. Nucleic Acids Res. 2015 Jan 28;43(D1):D413–22.

75. Van Dijk MR, Janse CJ, Thompson J, Waters AP, Braks JAM, Dodemont HJ, et al. A Central Role for P48/45 in Malaria Parasite Male Gamete Fertility The central role of zygote formation in the life cycle and transmission of the parasite makes gametes and. Vol. 104, Cell. 2001.

76. KUMAR Nirbhay. Target antigens of malaria transmission blocking immunity exist as a stable membrane bound complex. Vol. 9, Parasite Immunology. 1987.
77. Farrance CE, Rhee A, Jones RM, Musiychuk K, Shamloul M, Sharma S, et al. A plant-produced Pfs230 vaccine candidate blocks transmission of Plasmodium falciparum. Clinical and Vaccine Immunology. 2011 Aug;18(8):1351–7.
78. Ponnudurai T, Lensen AHW, Van Gemert GJA, Bensink MPE, Bolmer M, Meuwissen JHET. Infectivity of cultured Plasmodium falciparum gametocytes to mosquitoes. Parasitology. 1989;98(2):165–73.
79. de Jong RM, Singh SK, Teelen K, van de Vegte-Bolmer M, van Gemert GJ, Stone WJR, et al. Heterologous Expression and Evaluation of Novel Plasmodium falciparum Transmission Blocking Vaccine Candidates. Front Immunol. 2022 Jun 23;13.
80. de Jong RM, Alkema M, Oulton T, Dumont E, Teelen K, Nakajima R, et al. The acquisition of humoral immune responses targeting Plasmodium falciparum sexual stages in controlled human malaria infections. Front Immunol. 2022 Jul 18;13.
81. Meerstein-Kessel L, Van Der Lee R, Stone W, Lanke K, Baker DA, Alano P, et al. Probabilistic data integration identifies reliable gametocyte-specific proteins and transcripts in malaria parasites. Sci Rep. 2018 Dec 1;8(1).
82. Staples TL. Expansion and evolution of the R programming language. R Soc Open Sci. 2023 Apr 12;10(4).
83. Ritchie ME, Phipson B, Wu D, Hu Y, Law CW, Shi W, et al. Limma powers differential expression analyses for RNA-sequencing and microarray studies. Nucleic Acids Res. 2015 Jan 6;43(7):e47.
84. Punjani A, Rubinstein JL, Fleet DJ, Brubaker MA. cryoSPARC: algorithms for rapid unsupervised cryo-EM structure determination. Nature Methods 2017 14:3 [Internet]. 2017 Feb 6 [cited 2023 Oct 22];14(3):290–6. Available from: https://www.nature.com/articles/nmeth.4169
85. Vonrhein C, Flensburg C, Keller P, Sharff A, Smart O, Paciorek W, et al. Data processing and analysis with the autoPROC toolbox. Acta Crystallogr D Biol Crystallogr. 2011 Apr;67(4):293–302.
86. Kabsch W. *XDS*. Acta Crystallogr D Biol Crystallogr [Internet]. 2010 Feb 1;66(2):125–32. Available from: https://scripts.iucr.org/cgi-bin/paper?S0907444909047337
87. McCoy AJ, Grosse-Kunstleve RW, Adams PD, Winn MD, Storoni LC, Read RJ. Phaser crystallographic software. J Appl Crystallogr. 2007 Jul 13;40(4):658–74.
88. Liebschner D, Afonine P V., Baker ML, Bunkoczi G, Chen VB, Croll TI, et al. Macromolecular structure determination using X-rays, neutrons and electrons: Recent developments in Phenix. Acta Crystallogr D Struct Biol. 2019 Oct 1;75:861–77.
89. Emsley P, Lohkamp B, Scott WG, Cowtan K. Features and development of Coot. Acta Crystallogr D Biol Crystallogr. 2010;66(4):486–501.

90. Krissinel E, Henrick K. Inference of Macromolecular Assemblies from Crystalline State. J Mol Biol. 2007 Sep 21;372(3):774–97.
91. Goddard TD, Huang CC, Meng EC, Pettersen EF, Couch GS, Morris JH, et al. UCSF ChimeraX: Meeting modern challenges in visualization and analysis. Protein Science. 2018 Jan 1;27(1):14–25.
92. Pettersen EF, Goddard TD, Huang CC, Meng EC, Couch GS, Croll TI, et al. UCSF ChimeraX: Structure visualization for researchers, educators, and developers. Protein Science. 2021 Jan 1;30(1):70–82.

1157 **Figures and Tables:**
1158
1159
1160

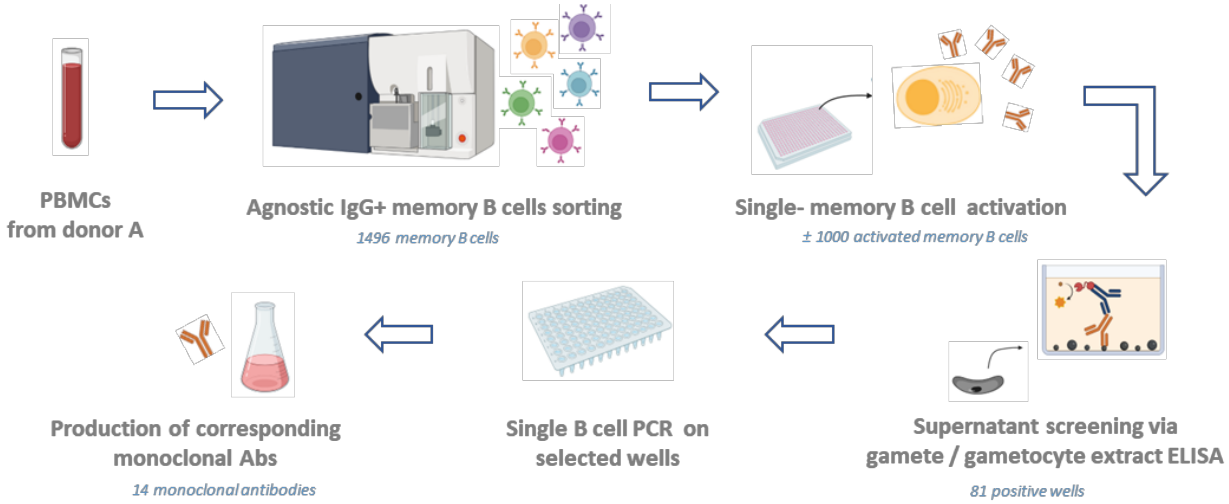

1161
1162 **Figure 1: General workflow.** IgG+ memory B cells from Donor A were sorted individually
1163 regardless of their specificity, at one cell per well. Cells were further cultured in activation medium
1164 with CD40L-expressing feeder cells and cytokines to induce antibody secretion. Supernatants
1165 were tested for antibody binding to the sexual stage of the parasite through screening using a
1166 gamete extract ELISA. Memory B cells from wells displaying reactivity were selected for Ig genes
1167 amplification, followed by cloning and production of the corresponding antibody. Figure was
1168 created with Biorender.
1169

A

	% pos wild-type gametes			% pos Pfs48/45 knock-out gametes		
	100 µg/ml	5 µg/ml	1 µg/ml	100 µg/ml	5 µg/ml	1 µg/ml
B1C5L	77.5	82.7	92.5	7.2	1.6	1.0
B1C5K	68.7	92.3	94.8	3.0	2.0	1.8
B2C10L	66.5	58.6	68.9	3.1	4.0	4.6
B2E9L	76.2	75.3	82.3	11.3	9.9	9.7
B1C8L	60.7	2.5	2.0	2.1	1.0	1.0
B1C8K	10.5	1.0	0.8	3.8	0.6	1.3
B1D3L	3.0	2.0	2.0	6.4	1.1	0.7
B1D3K	4.9	3.5	2.6	8.6	2.8	1.9
B1F9K	1.5	1.9	2.0	1.0	0.8	0.9
B1E7K	60.9	2.8	1.1	5.6	1.5	1.0
B1C3L	2.8	1.0	1.1	3.5	1.7	1.5
B2D10L	49.5	61.7	17.2	4.2	4.2	5.0
B2F7L	18.5	9.5	3.8	5.5	4.7	5.3
B1E11K	27.8	30.0	19.0	18.8	18.8	19.9

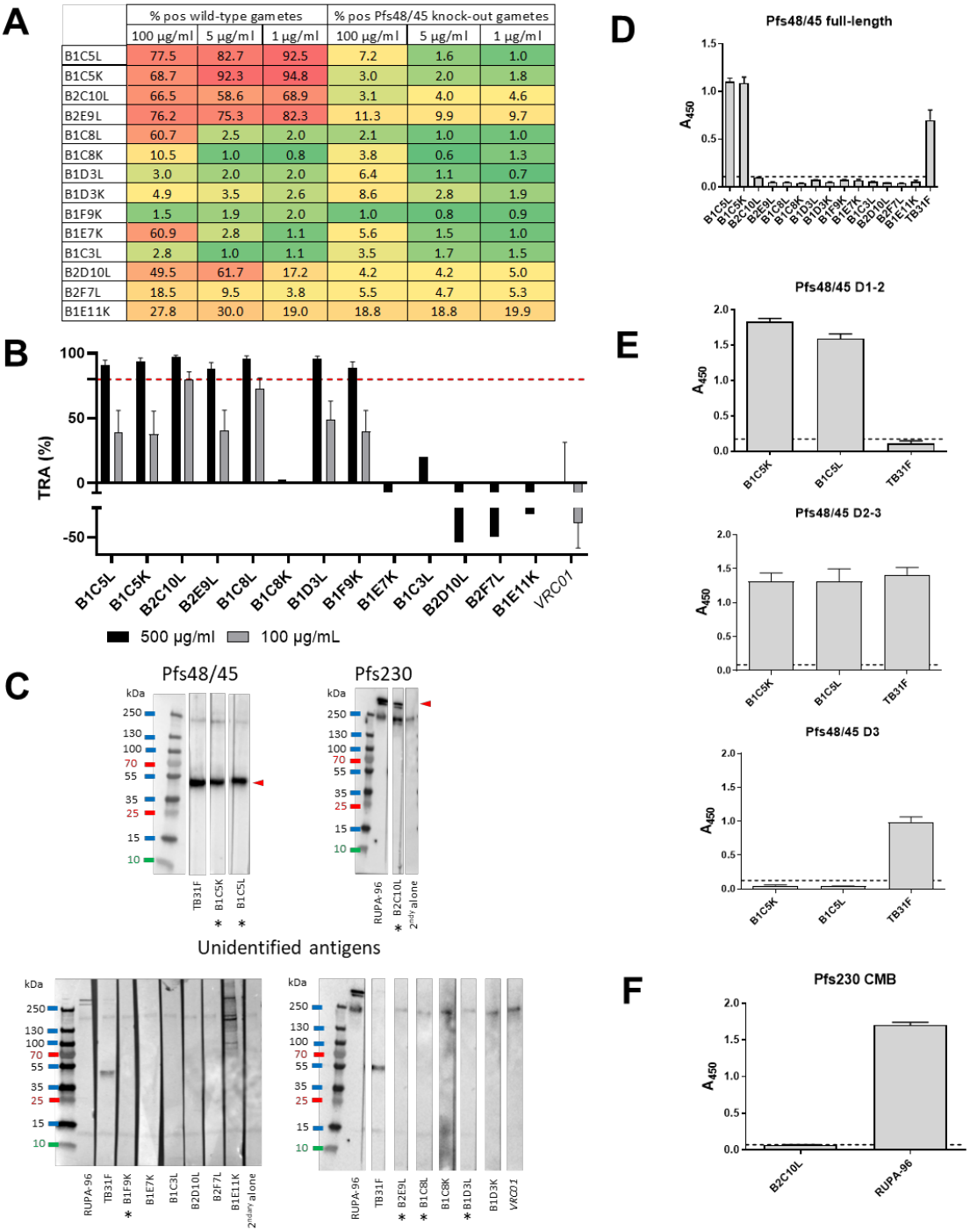

Figure 2: Characterization of the panel of isolated monoclonal antibodies. (A) Percentage positive wild-type gametes and Pfs48/45 knock-out (KO) gametes that also lack surface bound Pfs230 in surface immunofluorescence assay, in a heatmap format (graded color scale: red for high percentage of binding, green for low percentage of binding). The experiment was performed in duplicate and three different monoclonal antibody concentrations were tested (100 µg/ml, 5 µg/ml and 1µg/ml). (B) Transmission reducing activity (TRA) of the mAb panel in standard membrane feeding assay (SMFA). For mAbs with >80% TRA at 500 µg/ml, experiments were run in duplicates and bars are estimates of the mean and error bars represent the 95% confidence

1179 intervals. mAbs with >80% TRA at 500 µg/ml were also tested at 100 µg/ml. Oocyst count data of
1180 the SMFA experiments can be found in Table S2. (C) Reactivity of the monoclonal antibody panel
1181 against gametocyte extract in Western blot, in non-reducing conditions. Antibodies are classified
1182 depending on the antigen recognized: Pfs48/45, Pfs230, or no antigen identified. TB31F is an
1183 anti-Pfs48/45 monoclonal antibody, RUPA-96 is an anti-Pfs230 monoclonal antibody, and VRC01
1184 is an anti-HIV monoclonal antibody (negative control). Pfs48/45 and Pfs230 bands are indicated
1185 with a red arrow Antibodies with >80% TRA at 500 µg/ml are indicated with an asterisk (*). (D)
1186 Reactivity of the monoclonal antibody panel against full-length Pfs48/45 at 30 µg/ml in ELISA. (E)
1187 B1C5K and B1C5L binding to various Pfs48/45 domains in ELISA, at 10 µg/ml. (F) B2C10L
1188 binding to Pfs230 CMB domain in ELISA, at 10 µg/ml.

A

Peptide ID	Corresponding protein	Peptide position in the protein *Peptide length*	Normalised score	Corrected score
PF3D7_0220000	Liver Stage Antigen 3	67 to 822 *756*	6.253495	59988.5
PF3D7_0309100	OMD protein	Full length *187*	6.188559	57356
PF3D7_1149200	ring infected erythrocyte surface antigen 3 (RESA3)	65 to 587 *523*	6.193454	54235.5
PF3D7_0102200	ring infected erythrocyte surface antigen (RESA)	568 to 1085 (end) *518*	6.044558	53268
PF3D7_1127500	Protein disulfide isomerase	Full length *433*	5.913398	44843.5
PF3D7_1036300	Duffy binding like merozoite surface protein 2	423 to 762 *340*	5.433248	32032.5
PF3D7_0411700	conserved plasmodium protein	138	5.111879	25673.5
PF3D7_1038400	Pf 11.1	2980 to 3637 *658*	4.763914	21787
PF3D7_1149200	ring infected erythrocyte surface antigen 3	570 to 1090 *521*	4.723332	20946.5
PF3D7_0804500	uncharacterized protein	215	4.610963	19703
PF3D7_1038400	Pf 11.1	8737 to 9663 (end) *827*	3.986108	12776.5
PF3D7_1038400	Pf 11.1	7795 to 8628 *778*	3.757038	11117.5
PF3D7_0909000	uncharacterized protein	528	3.689088	10267
PF3D7_1038400	Pf 11.1	103 to 1024 *922*	3.242688	7017
PF3D7_0522400	uncharacterized protein	934	3.164308	6643.5

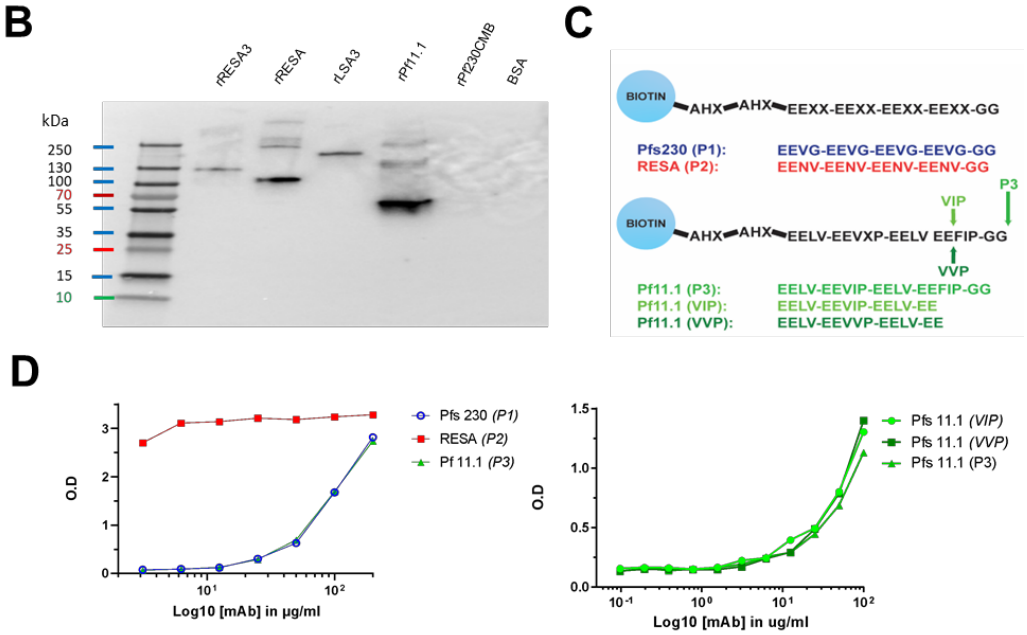

Figure 3: B1E11K binds repeat peptides. (A) B1E11K binding to recombinant fragments of Pf proteins displayed on a microarray. (B) B1E11K binding to several recombinant proteins in Western blot, in non-reducing conditions. (C) Sequences of the peptides tested for binding. Peptides were N-terminally linked to a biotin moiety using aminohexanoyl (Ahx) spacers. (D) B1E11K binding in ELISA to a panel of peptides.

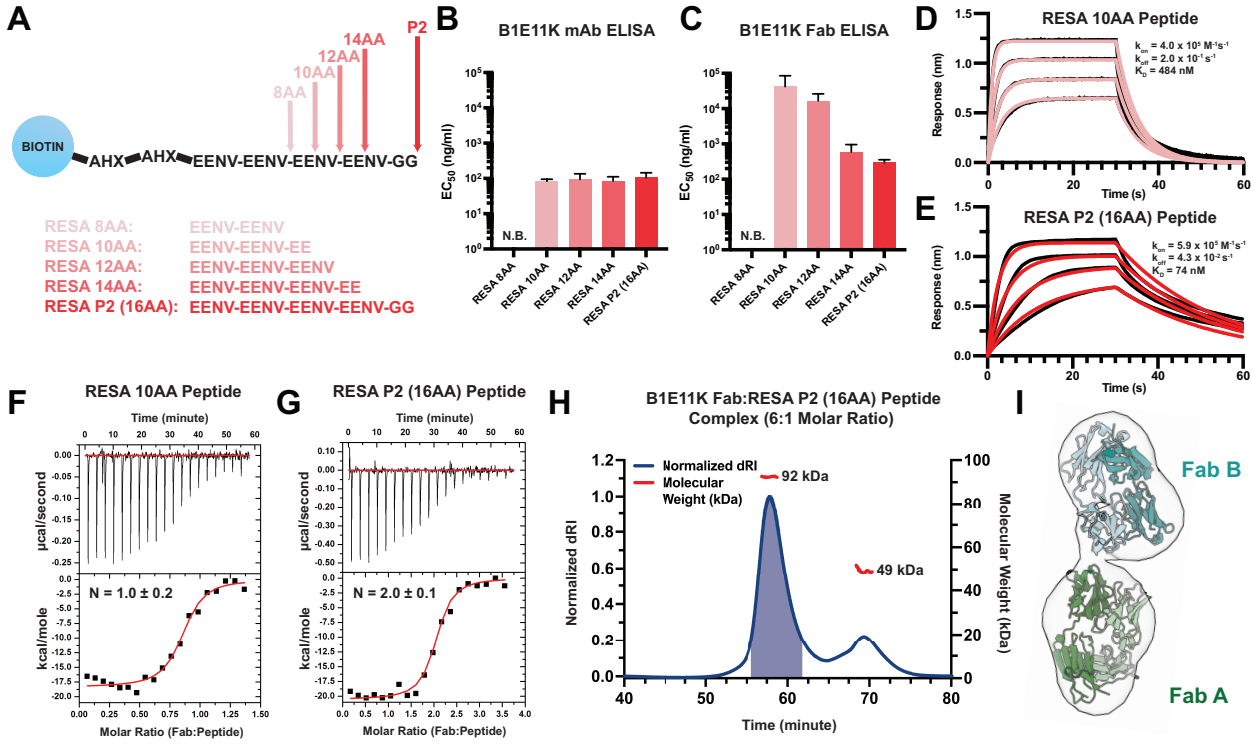

Figure 4: Binding Characteristics of RESA peptides to B1E11K. (A) Various peptides based on the EENV repeat region were designed and conjugated to a biotin-AHX-AHX moiety (AHX = ε-aminocaproic acid). EC_{50} values obtained from ELISA experiments utilizing various EENV repeat peptides with (B) B1E11K mAb or (C) B1E11K Fab. Error bars represent standard deviation. Biolayer interferometry experiments utilizing immobilized (D) RESA 10AA peptide or (E) RESA P2 (16AA) peptide dipped into B1E11K Fab. Representative isothermal titration calorimetry experiments in which B1E11K Fab was injected into (F) RESA 10AA peptide or (G) RESA P2 (16AA) peptide. (H) Size-exclusion chromatography coupled with multi-angle light scattering (SEC-MALS) of a solution of B1E11K Fab incubated with RESA P2 (16AA) peptide in a 6:1 molar ratio. The predicted molecular weight of the B1E11K Fab and RESA P2 peptide are 46.9 kDa and 2.5 kDa respectively. The shaded region indicates the fractions collected used for negative stain electron microscopy. (I) A nsEM map reconstruction which permits the fitting of two B1E11K Fabs (Fab A and Fab B).

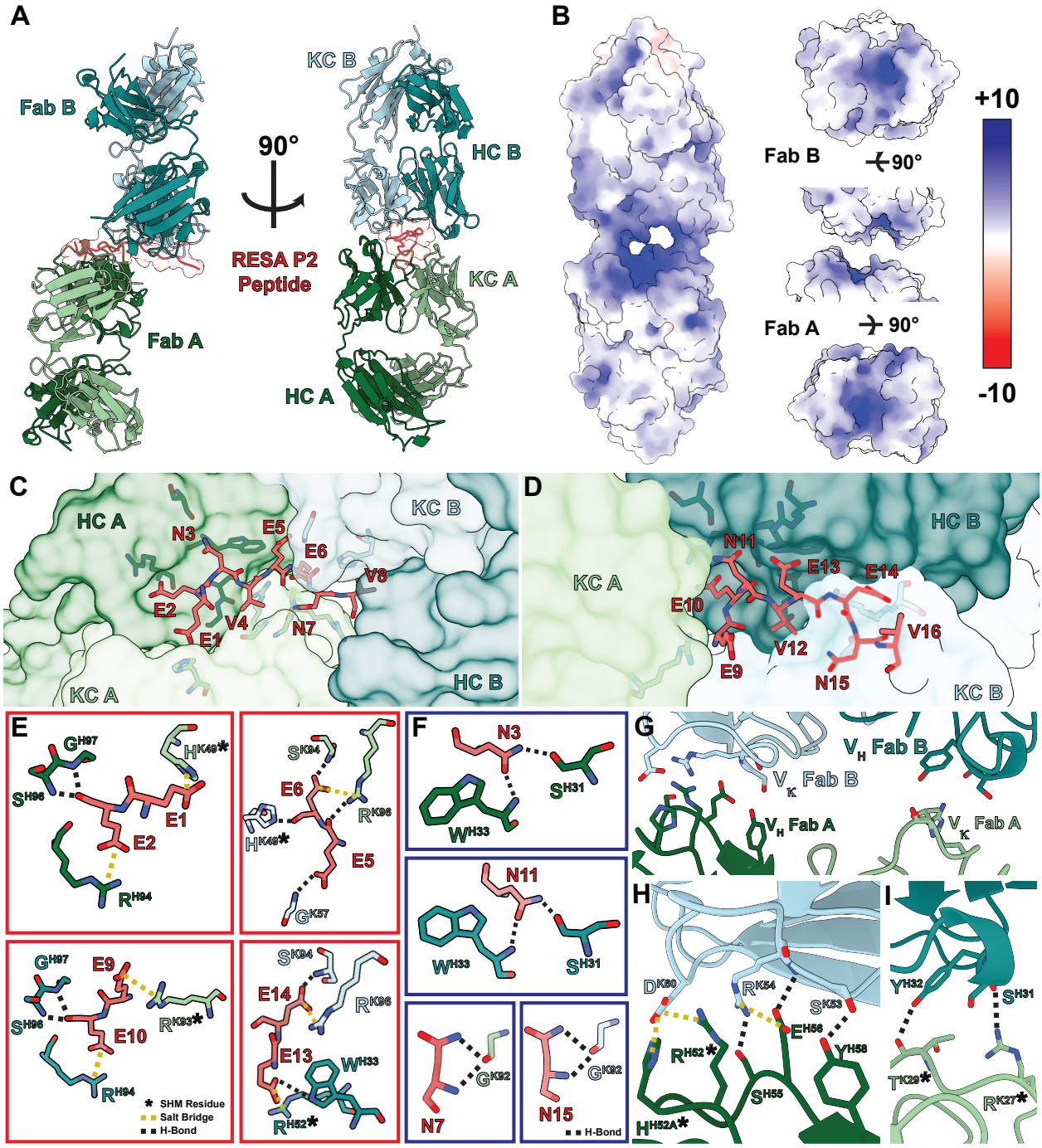

Figure 5: Structure of the B1E11K Fab and RESA P2 (16AA) peptide complex. (A) The overall architecture of the B1E11K:RESA P2 (16AA) peptide complex. (B) The electrostatic potential of the surface of the B1E11K Fabs. Fab residues involved in electrostatic interactions with (C) residues 1-8 and (D) 9-16 of the RESA P2 peptide are shown as sticks. (E) Electrostatic interactions occurring with glutamate residues of the RESA P2 (16AA) peptide. Residues that have undergone somatic hypermutation (SHM) are marked with an asterisk. Salt bridges are shown as dashed yellow lines and hydrogen bonds as dashed black lines. (F) Hydrogen bonding interactions through the asparagine residues of the RESA P2 (16AA) peptide are shown as black dashed lines. (G) Variable heavy (V_H) and variable kappa (V_κ) residues involved in homotypic interactions are shown as sticks. (H) The first interaction interface and (I) second interface.

1221 Residues that have undergone somatic hypermutation (SHM) are marked with an asterisk.
1222 Electrostatic interactions are presented as dashed lines and coloured as done previously.
1223
1224

1225 **Table 1: ITC thermodynamics and binding affinity of B1E11K Fab to RESA peptides.**

	RESA 10AA peptide (n=2)	RESA P2 peptide (n=3)
N	1.0 ± 0.2	2.1 ± 0.1
K_D (nM)	78 ± 12	73 ± 21
ΔG (kcal/mole)	-9.7 ± 0.3	-9.8 ± 0.3
ΔH (kcal/mole)	-18.3 ± 0.1	-20.5 ± 0.1
-TΔS (kcal/mole)	8.6 ± 0.2	10.7 ± 0.3

1226 Error reported as standard deviation.
1227
1228

1229 **Table 2: Crystallography statistics.**

Crystal	B1E11K:RESA P2 (16AA) peptide
Beamline	APS-23-ID-B
Wavelength (Å)	1.0332
Space group	C 2 2 2_1
Cell dimensions	
a,b,c (Å)	78.7, 186.3, 131.5
α, β, γ (°)	90, 90, 90
Resolution (Å)[a]	40.0 - 2.53 (2.65 – 2.56)
No. molecules in ASU	1
No. of observations	236,070 (23,834)
No. unique observations	31,520 (3,067)
Multiplicity	7.5 (7.8)
R_{merge} (%)[b]	14.5 (222.8)
R_{pim} (%)[c]	5.7 (85.5)
<I/σI>	10.8 (1.0)
$CC_{1/2}$ (%)	99.7 (36.5)
Completeness (%)	99.8 (98.5)
Refinement Statistics	
Reflections used in refinement	31,512
Reflections used in R-free	1,575
Non-hydrogen atoms	6,781
Macromolecule	6,627
Water	130
Heteroatom	24
R_{work}[d] / R_{free}[e] (%)	21.5 / 24.5
Rms deviations from ideality	
Bond lengths (Å)	0.002
Bond angle (°)	0.48
Ramachandran plot	
Favoured regions (%)	96.0
Allowed regions (%)	3.8
Ramachandran outliers (%)	0.2
B-factors (Å^2)	
Wilson B-factor	65.5
Average B-factors	89.8
Average macromolecule	90.3
Average Heteroatom	83.1
Average water molecule	61.0

1230 [a]Values in parentheses refer to the highest resolution bin.
1231 [b]$R_{merge} = \Sigma_{hkl} \Sigma_i | I_{hkl,\,i} - \langle I_{hkl} \rangle | / \Sigma_{hkl} \langle I_{hkl} \rangle$
1232 [c]$R_{pim} = \Sigma_{hkl} [1/(N - 1)]^{1/2} \Sigma i | I_{hkl,\,i} - \langle I_{hkl} \rangle | / \Sigma_{hkl} \langle I_{hkl} \rangle$
1233 [d]$R_{work} = (\Sigma | |Fo| - |Fc| |) / (\Sigma | |F_o|)$ - for all data except as indicated in footnote e.
1234 [e]5% of data were used for the R_{free} calculation.
1235